NASA Technical Memorandum 102840

An Evaluation of Three Two-Dimensional Computational Fluid Dynamics Codes Including Low Reynolds Numbers and Transonic Mach Numbers

Raymond M. Hicks and Susan E. Cliff, Ames Research Center, Moffett Field, California

January 1991

NASA
National Aeronautics and
Space Administration

Ames Research Center
Moffett Field, California 94035-1000

NOMENCLATURE

c	airfoil chord, in.
c_d	section drag coefficient
c_l	section lift coefficient
c_m	section pitching moment coefficient referenced to quarter chord
C_p	pressure coefficient $(p_\ell - p_\infty)/q_\infty$
h	tunnel height, ft
p	static pressure, lb/ft^2
q	dynamic pressure, lb/ft^2
Re	Reynolds number based on free-stream conditions and airfoil chord
x	airfoil abscissa, in.
y	airfoil ordinate, in.
α	angle of attack, deg
$\Delta\alpha$	angle-of-attack correction, deg
δ	correction factor

Subscripts

ℓ	local
∞	free-stream conditions

SUMMARY

Full-potential, Euler, and Navier-Stokes computational fluid dynamics (CFD) codes were evaluated for use in analyzing the flow field about airfoil sections operating at Mach numbers from 0.20 to 0.60 and Reynolds numbers from 500,000 to 2,000,000. The potential code (LBAUER) includes weakly coupled integral boundary-layer equations for laminar and turbulent flow with simple transition and separation models. The Navier-Stokes code (ARC2D) uses the thin-layer formulation of the Reynolds-averaged equations with an algebraic turbulence model. The Euler code (ISES) includes strongly coupled integral boundary-layer equations and advanced transition and separation calculations with the capability to model laminar separation bubbles and limited zones of turbulent separation. The best experiment/CFD correlation was obtained with the Euler code because its boundary-layer equations model the physics of the flow better than the other two codes. An unusual reversal of boundary-layer separation with increasing angle of attack, following initial shock formation on the upper surface of the airfoil, was found in the experimental data. This phenomenon was not predicted by the CFD codes evaluated during this study.

INTRODUCTION

Low-Reynolds-number airfoil design has presented challenging problems to the aircraft designer for many years. The most difficult of these design problems is predicting the increase in the profile drag of the airfoil that results from laminar separation bubbles. The drag caused by the bubbles becomes significant at Reynolds numbers below 500,000. Proper shaping of the camber and thickness distribution can reduce the size of the separation bubbles and provide a transition mechanism before strong adverse pressure gradients develop. Extensive research has been devoted to the development of efficient airfoils for low-speed flight at low Reynolds number. An excellent compilation of papers describing such research can be found in reference 1. However, very few transonic, low-Reynolds-number airfoil data are available.

Low-Reynolds-number airfoil design for transonic flight is more difficult than that for incompressible flow because of the high probability of developing shock waves on one or both surfaces of the airfoil. The strong adverse pressure gradients associated with the shocks and the effect of compressibility on the size and location of the bubbles complicates the design. The rapid movement of the shocks with changing Mach number and angle of attack renders a single airfoil shape of limited value in controlling the size and location of the separation bubbles.

New experimental facilities and new techniques for predicting transonic airfoil characteristics at low Reynolds numbers may be needed to address this problem. Most computational fluid dynamics (CFD) methods neglect the increase in growth of the momentum thickness through the laminar bubble, which results in a boundary layer that is too thin at the beginning of the turbulent boundary layer. This inadequacy increases the difficulty of low-Reynolds-number airfoil design because the designer must rely on approximate methods and experience to estimate the location and size of the bubbles.

This report evaluates three two-dimensional CFD codes in an effort to identify techniques capable of analyzing the flow field about arbitrary airfoils operating at transonic speeds and at low Reynolds numbers. One of the codes can model laminar separation bubbles. The airfoil section chosen for this code evaluation is designated LRN 1015. LRN stands for low Reynolds number and the first two digits following LRN give the design lift coefficient in tenths; the last two digits indicate the approximate maximum thickness/chord ratio in hundredths. Hence, the design lift coefficient of the LRN 1015 airfoil is 1.0 and the maximum thickness/chord ratio is 0.152. The airfoil was designed for a Mach number (M) of 0.55 and a Reynolds number (Re) of 500,000. The airfoil was tested in the 2- by 2-Foot Transonic Wind Tunnel at Ames Research Center.

DESCRIPTION

Model

A wind tunnel model of the LRN 1015 airfoil was machined from stainless steel; the model had a chord of 6 in. and a span of 24 in. Twenty-three orifices were drilled on the upper surface and 21 were drilled on the lower surface. The orifices were drilled normal to the upper and lower surfaces and were used in determining the surface-pressure distributions. The profile of the LRN 1015 airfoil section is shown in figure 1, and the coordinates are given in table 1.

Wind Tunnel

The test was conducted in the Ames 2- by 2-Foot Transonic Wind Tunnel, which is a variable-speed, continuous-flow, ventilated-wall, variable-pressure facility. The tunnel can be used for two-dimensional testing by replacing the ventilated side walls with solid glass walls that support the model. The glass walls were rotated by a motorized drive system to change the angle of attack. An 82-tube drag rake located 1.75 chords downstream from the trailing edge was used to survey the model wake. Airfoil models were mounted spanning the horizontal dimension of the tunnel test section, with the center of rotation of the side windows located near the 25%-chord station on the model. The gaps between the ends of the model and the side windows were sealed to improve the two-dimensionality of the flow.

Instrumentation

The model surface and wake rake pressures were measured by an automatic pressure-scanning system that uses precision pressure transducers. Basic tunnel pressures were measured with precision mercury manometers. The angle of attack was measured with a potentiometer operated by the drive gear for the rotating side windows. Data were obtained by a high-speed data-acquisition system.

Test

The aerodynamic characteristics of the airfoil were measured at Mach numbers of 0.20, 0.50, 0.55, and 0.60 and at nominal Reynolds numbers of 500,000, 1,000,000 and 2,000,000. The angles of attack ranged from approximately –6.0° to 18.0°, depending on Mach number and stalling angle of the model. The entire test was conducted with the wake rake installed since previous tests in the 2- by 2-foot tunnel showed that the effect of the wake rake on the model surface pressures is negligible for the rake position used in the present test. Data were obtained at all test conditions with free transition.

Pressure coefficients were determined from surface-pressure measurements. Section normal force and pitching-moment coefficients were obtained from an integration of the surface-pressure coefficients. The pitching-moment coefficients were referenced to the quarter chord. Profile drag was calculated from the wake-rake total and static-pressure measurements.

The model angle of attack was corrected for the presence of the tunnel walls by the following equation:

$$\Delta\alpha = \delta(c/h)c_l$$

where $\Delta\alpha$ is the angle-of-attack correction, δ is the angle-of-attack correction factor, c/h is the model chord/tunnel-height ratio, and c_l is the section lift coefficient. The correction factor δ is a function of Mach number. The angle-of-attack corrections ranged from 0.0° to over 3.0°, depending on Mach number and lift coefficient. Corrections of this magnitude cause the accuracy of the experimental angles of attack quoted in this report to be questioned. The large corrections are due in part to the use of a single plenum chamber surrounding the test section in the 2- by 2-foot tunnel. This type of plenum permits a reduction in the pressure difference between the upper and lower surfaces of the model, which, in turn, reduces the effective angle of attack of the model. Wind tunnels with separate plenums above and below the test section usually have smaller angle-of-attack corrections. The Mach number corrections resulting from the presence of the tunnel walls were negligible for the Mach numbers used in this investigation.

EXPERIMENT/CFD COMPARISONS AND DISCUSSION

Three CFD codes were used to calculate the flow field about the LRN 1015 airfoil. The Euler code ISES (ref. 2) solves the steady-state equations by a finite-volume discretization along with an H-grid in which one set of coordinate lines represent streamlines. This formulation reduces the equation set, thereby resulting in a more efficient code than those with the more traditional formulations. The equations are solved by Newton's method along with Gaussian elimination. The boundary layer and wake are strongly coupled to the inviscid flow field by solving an integral formulation of the boundary-layer equations simultaneously with the inviscid equations. This gives a precise modeling of the shock/boundary-layer interaction for transonic calculations and an accurate representation of laminar separation bubbles.

Three different views of the initial computational grid used with ISES are shown in figures 2–4. The grid cells are bunched in the vicinity of the airfoil with somewhat tighter clustering near the leading and trailing edges and at the surface, for boundary-layer resolution. The transition position is determined by an e^n method similar to that of Smith (ref. 3), which models the spatial growth rate of Tollmein-Schlichting waves, the assumed transition mechanism. The exponent n is a measure of the turbulence level of the flow. A value of 9 is reasonable for most flow conditions and a value of 16 to 18 is appropriate for a quiet atmosphere.

The Navier-Stokes code used during this study is ARC2D (ref. 4), a thin-layer formulation of the Reynolds-averaged equations using a Baldwin-Lomax turbulence model. Only limited computations with ARC2D were made, because the experiment/CFD correlations were inferior to those for ISES and execution of ARC2D required greater computational resources than ISES. The computational grid used with ARC2D is shown in figures 5–7. A C-grid was used in the wraparound streamwise direction, with strong bunching near the leading and trailing edges and at the surface. Note that the outer boundary is located much farther from the airfoil than for ISES (compare figs. 2 and 5).

The third code evaluated was a modified version of PROGRAM-H (ref. 5) designated LBAUER. This code solves the full-potential equation in nonconservative form by successive line overrelaxation, after conformally mapping the airfoil to the inside of a circle. Weakly coupled integral boundary-layer equations are used with LBAUER; that is, the boundary-layer equations are solved independently from the potential equation. The turbulent boundary-layer characteristics are calculated by the Nash-Macdonald method (ref. 6), and the laminar boundary layer is computed by the method of Thwaites. Transition and separation are determined by a simple pressure-gradient criterion. LBAUER was included because it has been used extensively by the aircraft community and is computationally efficient. Previous evaluations of LBAUER (ref. 7) have shown that the code can fairly accurately predict surface pressures for supercritical airfoils operating with attached flow at subsonic or transonic Mach numbers and at high Reynolds numbers. The current study considers Reynolds numbers that are well below the intended range of the LBAUER code.

ISES and LBAUER were used to calculate surface-pressure distributions and aerodynamic force and moment coefficients for the LRN 1015 airfoil at Mach numbers of 0.20, 0.50, 0.55, and 0.60 and at nominal Reynolds numbers of 500,000, 1,000,000 and 2,000,000. ARC2D computations are included for a limited subset of the test data. Computations are shown for selected lift coefficients from near zero to near stall. All experiment/CFD correlations are presented for matched lift coefficient, Mach number, and Reynolds number except as noted. Lift-coefficient matching was used because of the uncertainty in the experimental angles of attack. Most of the test conditions chosen for comparison with the computations had attached flow with short laminar separation bubbles on both surfaces. Some experimental data that show trailing-edge separation have been included to test the capability of the codes to model turbulent separation and to predict maximum lift coefficient. The convergence level for LBAUER, ISES, and ARC2D was, respectively, approximately a 10-, 9-, and 5-orders-of-magnitude reduction in an appropriate numerical quantity.

The surface-pressure distributions for Mach 0.20 are shown in figures 8–10 for selected lift coefficients. For this Mach number, the experimental pressure distributions are compared with computational results from LBAUER and ISES (ARC2D is not included). Both the LBAUER and ISES codes predict the general shape of the pressure distributions well for test conditions with attached flow. However the pressures computed using ISES exhibit laminar separation bubbles, whereas the pressures calculated by using LBAUER do not (e.g., see figs. 8(a) and 8(b)). Note that separation bubbles appear on both surfaces at most lift coefficients. The lower-surface bubble is usually located near the 80%-chord station except when leading-edge pressure peaks are present on the lower surface at low lift coefficients (e.g., fig. 9(a)). The upper-surface bubble moves forward with increasing angle of attack, denoting transition (fig. 9(e)).

A careful examination of the pressure distribution indicates that at some test conditions ISES predicts a different transition location than that shown by experiment. For example, at $c_l = 0.981$, the experimental transition position is located near x/c = 0.15, whereas ISES gives transition at x/c = 0.40 (fig. 9(d)). The experimental transition is more difficult to identify than the computational transition on the pressure distributions because the experimental bubble appears smaller and more diffuse than the computational bubble when the transition is located forward on the airfoil. The ability to predict the location, size, and drag of laminar separation bubbles is important for CFD codes, since laminar bubbles are responsible for an increasing part of the profile drag as the Reynolds number decreases below 500,000. The ISES computations indicate that transition from laminar to turbulent flow is usually accompanied by a separation bubble for the test cases shown here. Note that the experimental angle of attack listed on the figures is larger than the computational angles for most test conditions. The angle-of-attack corrections discussed earlier in the section on test procedures were determined by testing 3 models of the NACA 64A010 airfoil with chord lengths of 4.0, 6.0, and 8.0 in. and may not be applicable to arbitrary airfoil sections.

Note that LBAUER gives a more accurate representation of the pressure distribution at some test conditions near maximum lift than ISES does, when the trailing-edge pressure recovery is good; this indicates attached flow (e.g., fig. 8(e)). When trailing-edge separation is present the experiment/CFD correlation can be poor for both codes (e.g., fig. 9(f)) or good for ISES and poor for LBAUER (figs. 10(e) and 10(f)). It appears that ISES is capable of modeling trailing-edge separation for certain test conditions as long as the separation does not exceed 30% of the chord. More work is needed to understand why ISES accurately predicts trailing-edge separation at some test conditions and not at others. The free-air boundary conditions may be a source of error in the computations, and wall contamination of the model flow field may be a source of error in the experimental data at lift coefficients near stall. The reversal in the movement of separation with angle of attack is an indication that wind-tunnel effects may be present in the data. This reversal was documented during testing and will be discussed later.

The experiment/CFD correlations for Mach 0.50 are shown in figures 11–14. Navier-Stokes (ARC2D) computations are shown for selected test conditions at this Mach number. Note that the agreement between ARC2D and experiment is similar to that for LBAUER. Both codes are capable of predicting the location of boundary-layer separation, but neither code gives the correct surface-pressure distribution for separated regions. Velocity profiles calculated by ARC2D are shown in figure 12 for the test conditions of figure 11(e). Note that ARC2D shows reversed flow near the surface; this is consistent with the poor pressure recovery shown in the experimental data. However the ARC2D pressure distribution shown in figure 11(e) does not show the expected pressure plateau for the separated region near the trailing edge. The absence of a pressure plateau results from limited influence of the boundary layer on the outer flow, indicating that the computational zone of separation is too thin. A more advanced turbulence model or more grid clustering near the surface or both might improve the computation.

It is apparent that LBAUER gives the same degree of correlation with experiment as does ARC2D and does so with considerably less use of computational resources. Both codes give fairly good agreement with experiment for attached flow but are incapable of modeling separated flow. Since the objective is to avoid separation, there is little justification for using ARC2D in the design and analysis of airfoils for low-speed or transonic flight. There are, however, two advantages in using Navier-Stokes codes: (1) detailed velocity distributions in the boundary layer can be obtained,even though they may be somewhat inaccurate, and (2) the codes are valid for subsonic, transonic, and supersonic flow.

None of the three codes was capable of computing the separated flow near the trailing edge at Mach 0.50 and at a Reynolds number of 1,900,000 as shown in figures 14(f)–14(h). This means that reliable prediction of the maximum lift coefficient for an arbitrary airfoil is still not possible. The effect of free-stream turbulence level on the experiment/CFD correlation was examined by varying the exponent n in the e^n transition model in ISES. Calculations with n = 1 and n = 8 are shown for a lift coefficient of 1.215 in figures 14(g) and 14(h), respectively. Note that the computation with n = 1 gives slightly better correlation with test data over the last 30% of the airfoil, where separation is evident in the experimental pressures. However, a value of 1 for n indicates an unrealistically high level of turbulence in the 2- by 2-foot tunnel and, since the remainder of the experimental pressure distribution is poorly predicted by ISES there is no justification for using this low value for n. Note that when n is decreased from 8 to 1 the transition point moves from about 42% to 15% of the chord, consistent with a higher level of free-stream turbulence.

The experiment/CFD correlations for Mach 0.55 are shown in figures 15–17. Note that the lower-surface pressures are not accurately predicted by either LBAUER or ISES for the data with the negative lift coefficient shown in figure 15(a). The experiment/CFD correlations for the other test conditions at this Mach number are similar to those shown at the previous two Mach numbers, with ISES giving a more accurate prediction of the experimental pressures, primarily because of its ability to compute laminar separation bubbles (e.g., see fig. 16(c)). ISES is also slightly better at predicting pressures near the trailing edge on both surfaces than LBAUER at most test conditions, a result of a more accurate representation of the boundary layer. Note that the ISES computation agrees well with the experimental pressure distribution with separated flow over the last 30% of the chord at a Reynolds number of 1,000,000 (fig. 16(f)).

Poor agreement between computational and experimental pressures is again noted at lift coefficients above 1.0 in figures 17(d)–17(h). It is apparent that ISES would predict a maximum lift coefficient that is too high since attached flow is predicted at all lift coefficients, with the possible exception of $c_l = 1.400$ (fig. 17(h)). At this lift coefficient ISES indicates the poor trailing-edge pressure recovery consistent with separated flow but shows poor correlation with experimental pressures over the remainder of the upper surface. As noted earlier, the correlation of ISES computations with experiment for separated flow is sporadic and may indicate that wind-tunnel effects need more careful examination. As noted earlier, LBAUER gives excessive pressure recovery at the trailing edge at all test conditions, which indicates a thinner boundary layer than either ISES or experiment.

The experiment/CFD correlations for Mach 0.60 are shown in figures 18–20. Poor correlation is observed at low lift coefficients(figs. 18(a) and 18(b)). The inaccurate computations at these low lift coefficients is due to extensive flow separation on the lower surface, as indicated by the poor trailing-edge pressure recovery in the test data. The pressures computed by ISES again show slightly better correlation than those of LBAUER with experimental data at higher lift coefficients, because ISES models laminar separation bubbles (e.g., fig. 18(f), $c_l = 0.785$). The lower-surface separation bubble predicted by ISES is a little too far forward at this lift coefficient. The predicted bubble position is more accurate at a lift coefficient of 0.922 (fig. 18(g)). Note that ISES correctly predicts the pressure distributions with separated flow at some test conditions (figs. 18(i), 19(g), and 20 (f)) but fails to predict separation at others (figs. 20(d), 20(e), and 20(g)).

The hypothesis that wind-tunnel effects are responsible for the sporadic correlation of ISES computations with experiment for separated flow finds some support in the unusual separation trend with lift coefficient shown in figures 21–23. The surface-pressure distributions for lift coefficients approaching maximum lift for Mach 0.60 are shown in figure 21. Note that the pressure recovery near the trailing edge for the three lift coefficients shown for a Reynolds number of 500,000 (fig. 21(a)) shows the expected trend of decreasing pressure coefficients with increasing lift coefficient. This trend indicates an increasing boundary-layer thickness, with possible separation as the lift coefficient increases. However the variation of aft airfoil pressure coefficient with lift coefficient shows a reversal for Reynolds numbers of 1,000,000 and 2,000,000 (figs. 21(b) and 21(c)).

This unusual trend is clearly evident in figure 22, where the pressure coefficient at $x/c = 0.95$ on the upper surface is shown as a function of angle of attack for all test Mach numbers. Note that the pressure coefficient at this chord station becomes increasingly negative with increasing angle of attack for Mach numbers of 0.20 and 0.50 but shows a reversal for Reynolds numbers of 1,000,000 and 2,000,000 at Mach 0.55 and 0.60. The reversal is most evident at Mach 0.60. This phenomenon appears to be related to shock formation on the upper surface, as shown in figure 23, where the pressure coefficient curve of figure 22(d) for a Reynolds number of 2,000,000 is repeated along with pressure distributions at selected angles of attack. Note that the pressure distributions near angles of attack of 2.0° and 3.0° show upper-surface pressure plateaus near the trailing edge, which are indicative of separated flow. However, the pressure distribution at an angle of attack of 4° has a shock on the upper surface, better pressure recovery, and a more positive pressure coefficient at $x/c = 0.95$, indicating boundary-layer reattachment or at least a smaller zone of separation.

The acceleration of the flow downstream of the shock may be the mechanism causing a re-energized boundary layer and a temporary reduction in the extent of flow separation. If a separation bubble exists at the foot of the shock, an additional pressure recovery will occur downstream of the attachment point, causing a local acceleration of the flow as the boundary layer returns to equilibrium. The shocks occurring at angles of attack above 4.0° have sufficient strength to again cause forward movement of separation as well as a normal variation of aft pressure coefficient with angle of attack. The lack of separation reversal at a Reynolds number of 500,000 at Mach 0.60 may result from shock formation occurring with reduced strength at a higher angle of attack owing to the decambering of the airfoil by the thicker boundary layer. Further testing of this airfoil in another facility would be helpful in understanding the importance of the wind tunnel as a cause of the separation reversal.

The computational and experimental aerodynamic force and moment coefficients are shown in figure 24 for all test conditions selected for this evaluation. The experiment/CFD correlation at Mach 0.20 and at a Reynolds number of 500,000 shows that the LBAUER and ISES computations give similar agreement with the test data (fig. 24(a)). The correlations for Mach 0.20 at Reynolds numbers of 1,000,000 and 1,900,000 show that at higher lift coefficients, the ISES computations for the lift-curve agree more closely with the experimental data than the LBAUER computations do, because of a more accurate representation of the boundary layer (figs. 24(b) and 24 (c)). Computational results were not obtained for angles of attack much beyond the first bend in the lift-curves because the LBAUER computations do not give reliable results at these angles of attack and because ISES and ARC2D do not converge for extensive flow separation. Note that the ISES computations show a bend in the lift-curve consistent with the test data, whereas the LBAUER lift curve is linear, showing that the increase in boundary-layer thickness with angle of attack predicted by LBAUER is too small. The drag polars show similar differences between the codes, with ISES indicating the correct bend in the curve at moderate lift coefficients for the two higher Reynolds numbers. The experiment/CFD pitching-moment correlations for the two codes are similar except at the highest Reynolds number, where ISES follows the experimental curve better than LBAUER does (fig. 24(c)).

The force and moment comparisons for Mach 0.50 are shown in figures 24(d)–24(f). Computations obtained from ARC2D are compared with experiment and the other two codes at Reynolds numbers of 500,000 and 2,000,000 (figs. 24(d) and 24(f)). A close inspection of the figures shows that the ISES computations correlate slightly better than the other computations with the test data for lift and drag and that the ARC2D computations match the experimental pitching moment somewhat better at these Reynolds numbers. ARC2D computations were not obtained at a Reynolds number of 1,000,000 because the additional calculations were not justified by the correlations shown at the other Reynolds numbers.

The experiment/CFD correlations for Mach 0.55 show that the ISES predictions for lift and drag are slightly closer to the test data than the LBAUER calculations are at the three Reynolds numbers (figs. 24(g)–24(i)). However the LBAUER computations for pitching moment are slightly better than those of ISES at this Mach number. Note that ISES does not predict the first bend in the force and moment curves near a lift coefficient of 1.0 at a Reynolds number of 2,000,000 but does give the correct bend at a Reynolds number of 1,000,000 (compare figs. 24(h) and 24(i)). The irregular shape of the force and moment curves at high lift corresponds to the separation reversals discussed earlier. It is clear that the reversal in separation must be real and not a result of inaccurate surface-pressure measurements, since the drag is obtained from rake pressures in the wake and the lift and moment coefficients are determined by integration of surface pressures.

The aerodynamic force and moment data for Mach 0.60 (figs. 24(j)–24(l)) again show that the results of computations obtained from ISES correlate slightly better with the experimental results than do those of LBAUER. The improved experiment/CFD correlations for ISES are due to the correct modeling of limited zones of separation at low and high lift coefficients. Both codes give similar correlations with the test data for moderate lift coefficients where the boundary layer is attached.

CONCLUDING REMARKS

An experiment/CFD correlation was conducted to evaluate full-potential, Euler, and Navier-Stokes CFD codes for use in the analysis of airfoil sections for operation at low Reynolds numbers and at subsonic through transonic Mach numbers. Computations from the three codes were compared with test data for Reynolds numbers of 500,000, 1,000,000 and 2,000,000 at Mach numbers of 0.20, 0.50, 0.55, and 0.60. An Euler code with strongly coupled integral boundary-layer equations gave the best correlation with the experimental lift and drag data for test conditions with mild separation at low and high lift coefficients. The three codes gave similar correlations with the experimental lift curves over the linear range of the data. None of the codes showed a clear advantage for predicting pitching moment. The Euler code could predict the bend in the lift curves caused by the onset of flow separation for some test conditions but not for others. None of the codes was capable of predicting massive separation and hence could not calculate the maximum lift coefficients for this airfoil. The full-potential and Navier-Stokes codes could not predict the nonlinearities in the force and moment curves. An unusual reversal in the movement of trailing-edge separation with angle of attack, which was not predicted by any of the codes, was found in the test data.

REFERENCES

1. Aerodynamics at Low Reynolds Numbers ($10^4 < Re < 10^6$) International Conference. The Royal Aeronautical Society, London, England, Oct. 1986.

2. Giles, M.; Drela, M.; and Thompkins, W. T., Jr.: Newton Solution of Direct and Inverse Transonic Euler Equations. AIAA Paper 85-1530-CP, Cincinnati, OH, 1985.

3. Smith, A. M. O.; and Gamberoni, N.: Transition, Pressure Gradient, and Stability Theory. Report ES 26388, Douglas Aircraft Co., Long Beach, CA, 1956.

4. Pulliam, T. H.: Euler and Thin Layer Navier-Stokes Codes, ARC2D, ARC3D. U. of Tennessee Space Institute, Publication E02-4005-023-84, Tenn., 1984.

5. Bauer, Frances; Garabedian, Paul; and Korn, David: Supercritical Wing Sections. III. Lecture Notes in Economics and Mathematical Systems. Springer-Verlag, New York, 1977.

6. Nash, J. F.; and Macdonald, A. G. J.: The Calculation of Momentum Thickness in a Turbulent Boundary Layer at Mach Numbers up to Unity. Her Majesty's Stationery Office, C. P. No. 963, London, 1967.

7. Hicks, Raymond M.: An Assessment of a Modified Potential Flow Code for Calculating the Effect of Small Geometric Changes on the Pressures and Forces of Supercritical Airfoils. NASA TM-84287, 1982.

Table 1. LRN 1015 airfoil coordinates

Upper surface		Lower surface	
x/c	y/c	x/c	y/c
0.000000	0.000000	0.000000	0.000000
0.001621	0.017070	0.001621	–0.001976
0.006475	0.026197	0.006475	–0.004930
0.014529	0.036312	0.014529	–0.007513
0.025732	0.046990	0.025732	-0.010010
0.040010	0.057142	0.040010	–0.012525
0.057272	0.066677	0.057272	–0.014983
0.077405	0.075746	0.077405	–0.017226
0.100279	0.084202	0.100279	–0.019318
0.125745	0.092004	0.125745	–0.021214
0.153638	0.099088	0.153638	–0.022877
0.183777	0.105433	0.183777	–0.024304
0.215968	0.110974	0.215968	–0.025466
0.250000	0.115663	0.250000	–0.026357
0.285654	0.119458	0.285654	–0.026977
0.322698	0.122299	0.322698	–0.027302
0.360891	0.124114	0.360891	–0.027330
0.399987	0.124809	0.399987	–0.027065
0.439732	0.124264	0.439732	–0.026505
0.479867	0.122351	0.479867	–0.025652
0.520133	0.118919	0.520133	–0.024494
0.560268	0.113813	0.560268	–0.023028
0.600013	0.106947	0.600013	–0.021274
0.639109	0.098407	0.639109	–0.019239
0.677302	0.088455	0.677302	–0.016865
0.714346	0.077492	0.714346	–0.014081
0.750000	0.066230	0.750000	–0.010938
0.784032	0.055549	0.784032	–0.007663
0.816223	0.046102	0.816223	–0.004646
0.846362	0.037889	0.846362	–0.002130
0.874255	0.030724	0.874255	–0.000215
0.899721	0.024801	0.899721	0.001069
0.922595	0.020019	0.922595	0.001761
0.942728	0.015794	0.942728	0.001957
0.959990	0.011820	0.959990	0.001782
0.974268	0.008107	0.974268	0.001378
0.985471	0.004834	0.985471	0.000884
0.993525	0.002244	0.993525	0.000429
0.998379	0.000577	0.998379	0.000113
1.000000	0.000000	1.000000	0.000000

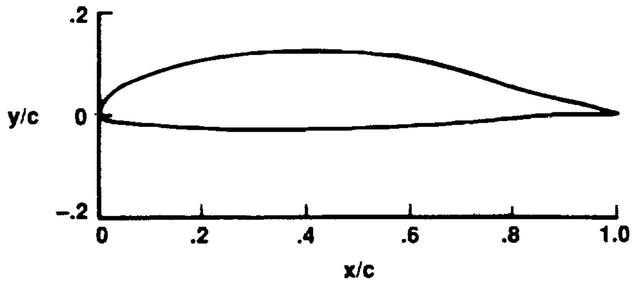

Figure 1. LRN 1015 airfoil: M = 0.55, c_l = 1.0, Re = 500,000 (design values).

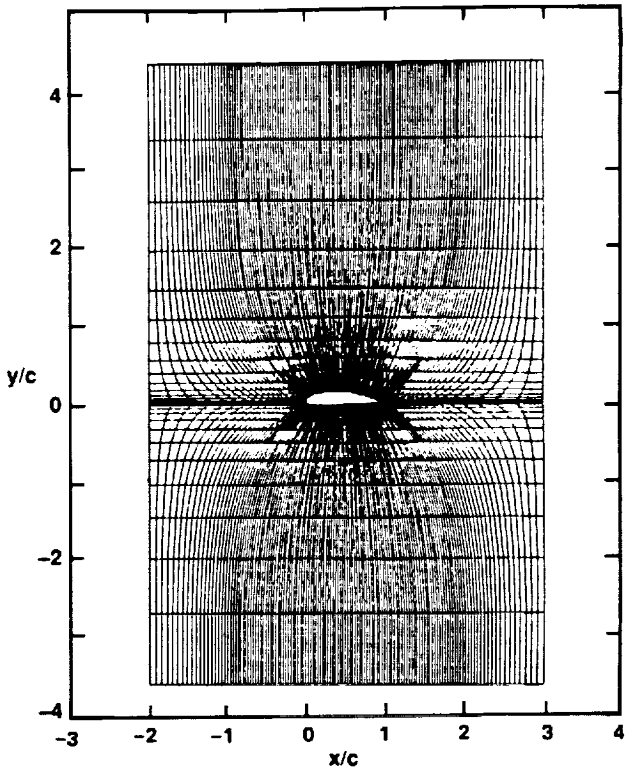

Figure 2. ISES computational grid (132 × 32) for LRN 1015 airfoil.

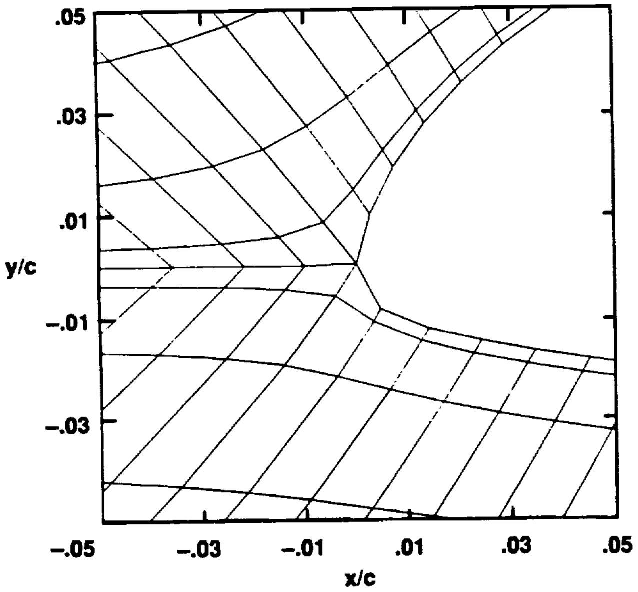

Figure 3. ISES computational grid near leading edge of LRN 1015 airfoil.

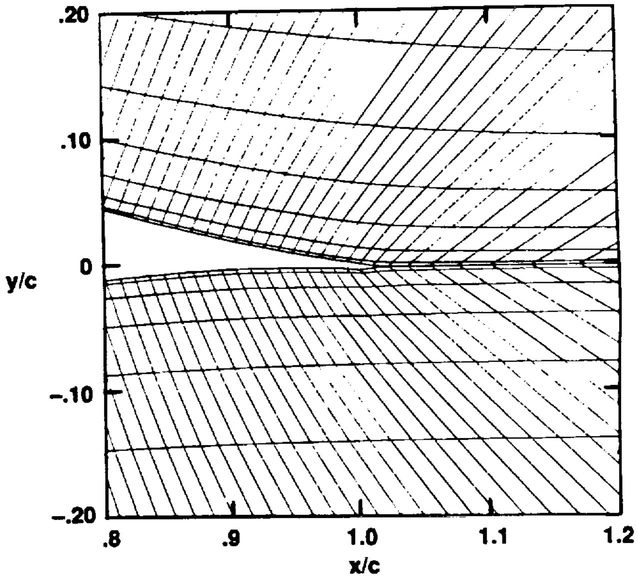

Figure 4. ISES computational grid near trailing edge of LRN 1015 airfoil.

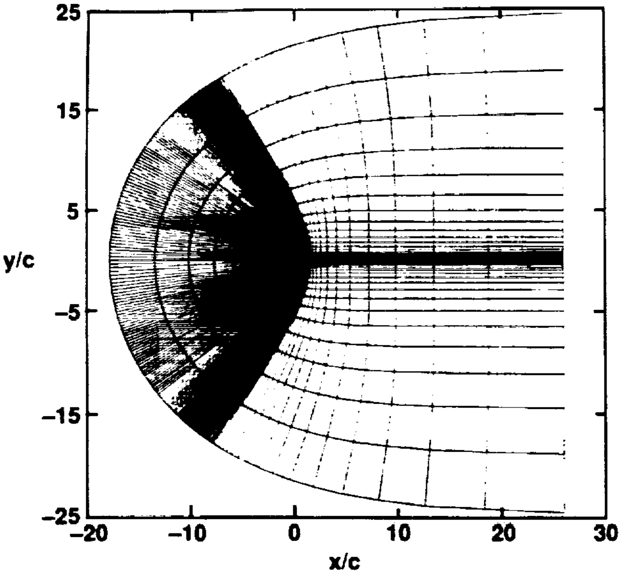

Figure 5. ARC2D computational grid (249 × 49) for LRN 1015 airfoil.

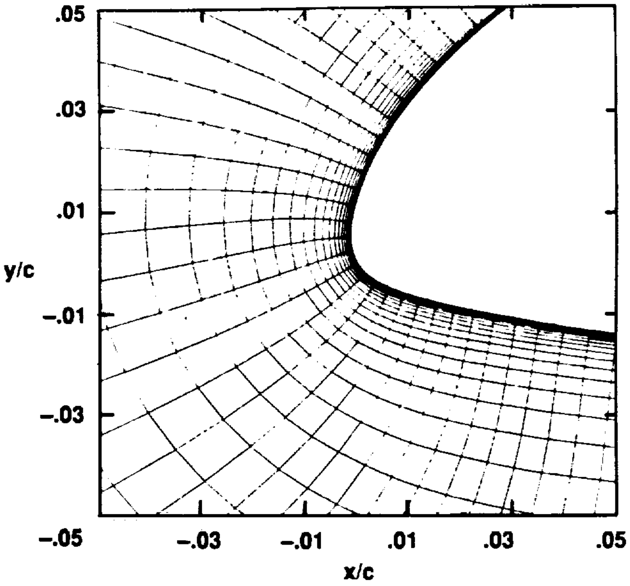

Figure 6. ARC2D computational grid near leading edge of LRN 1015 airfoil.

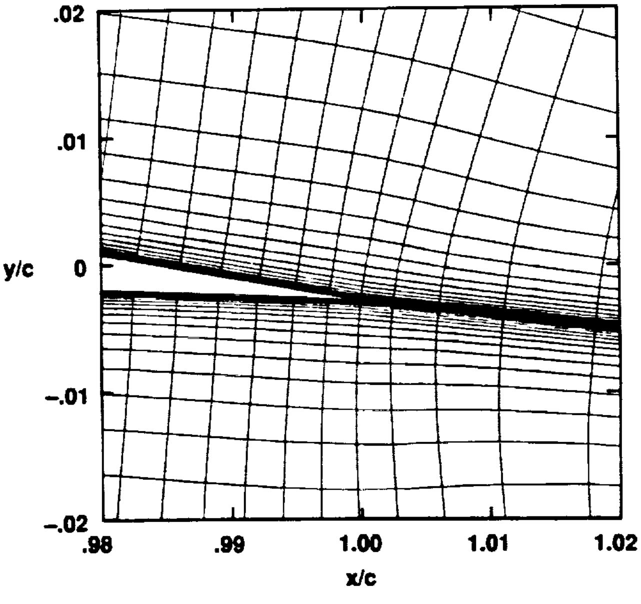

Figure 7. ARC2D computational grid near trailing edge of LRN 1015 airfoil.

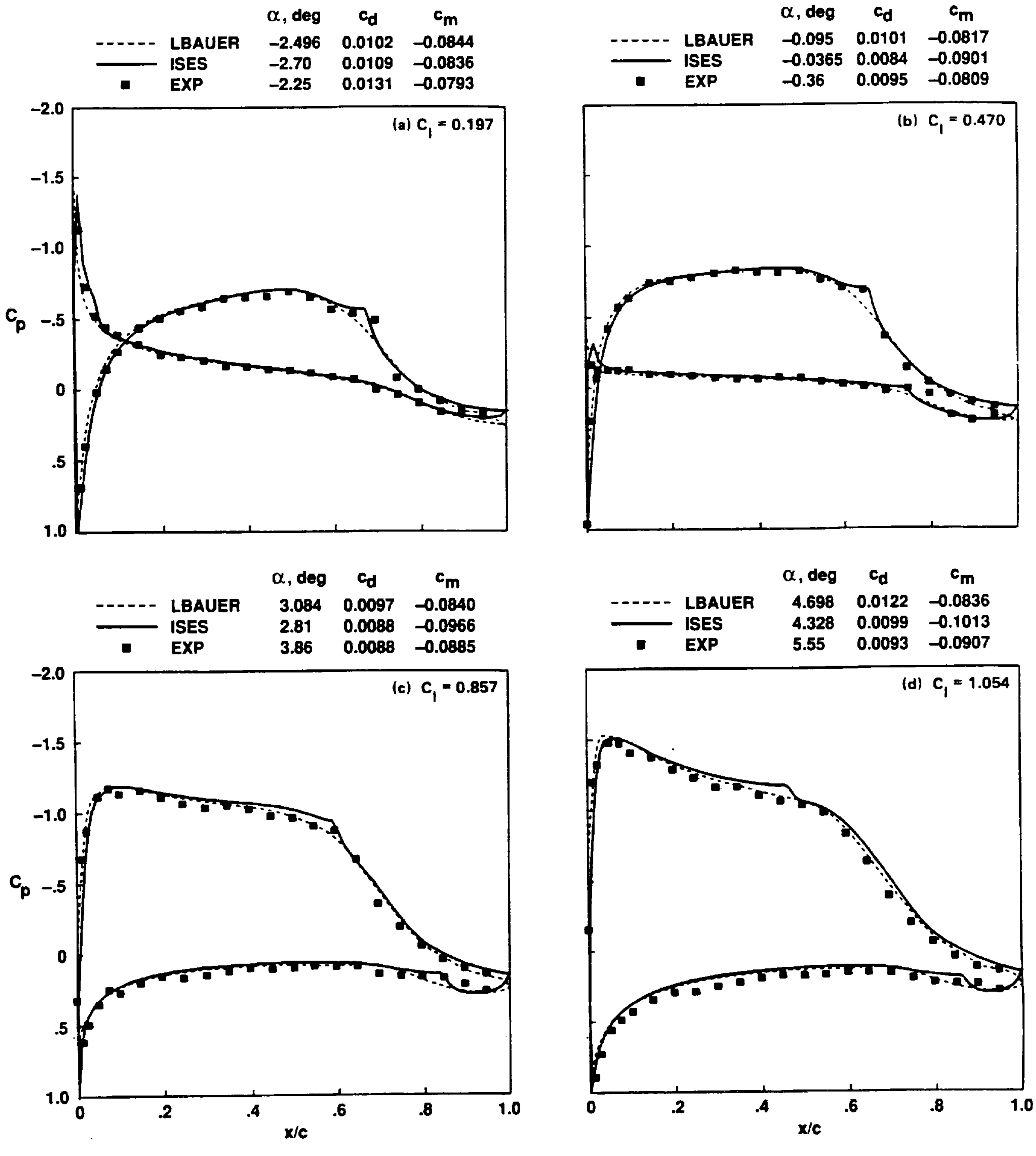

Figure 8. Surface-pressure distributions for LRN 1015 airfoil: M = 0.20, Re = 500,000.

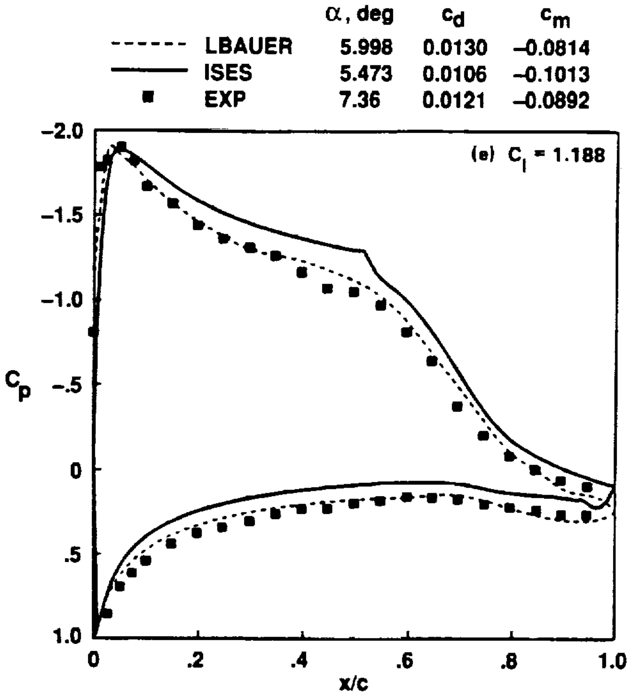

Figure 8. Concluded.

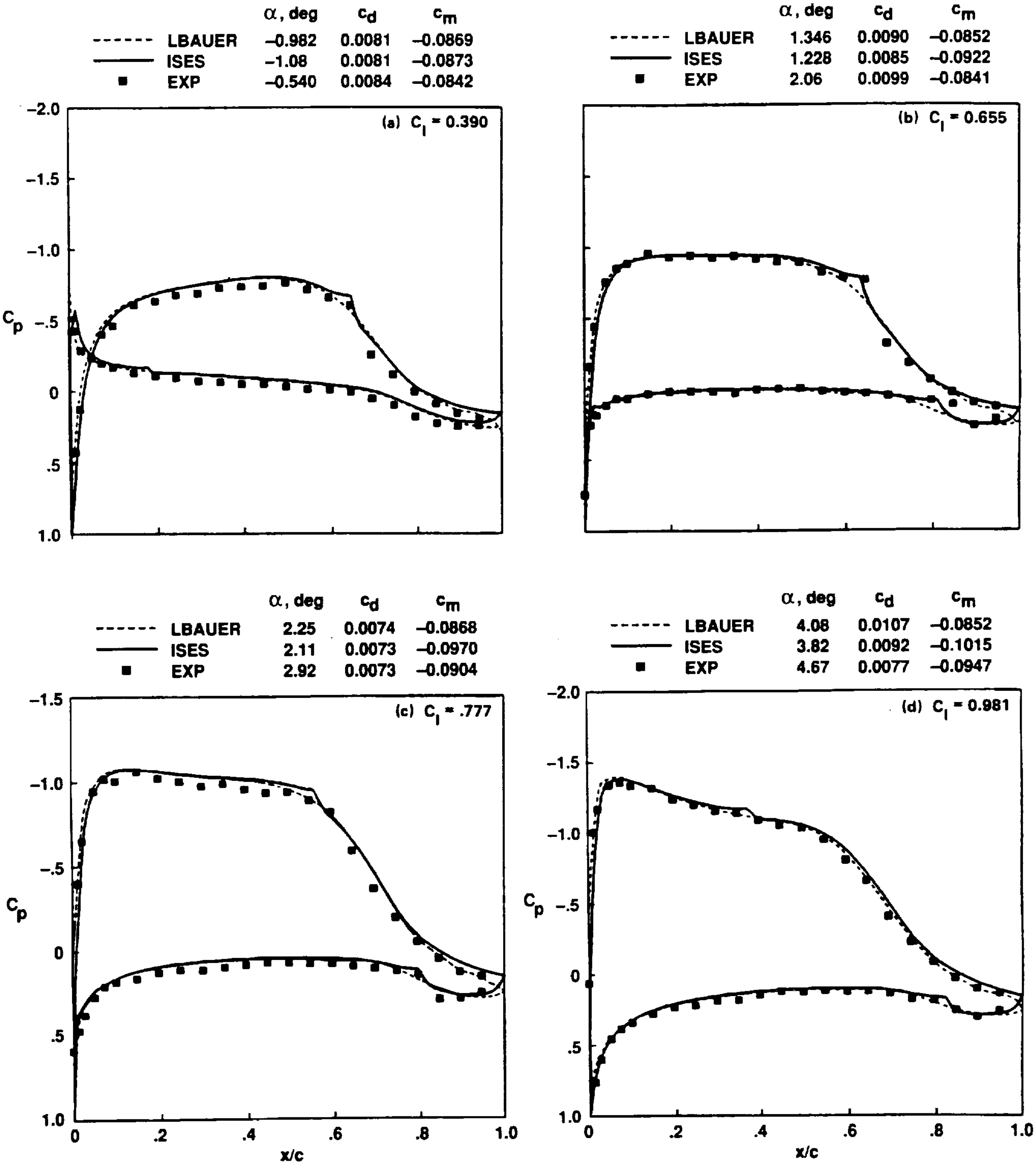

Figure 9. Surface-pressure distributions for LRN 1015 airfoil: M = 0.20, Re = 1,000,000.

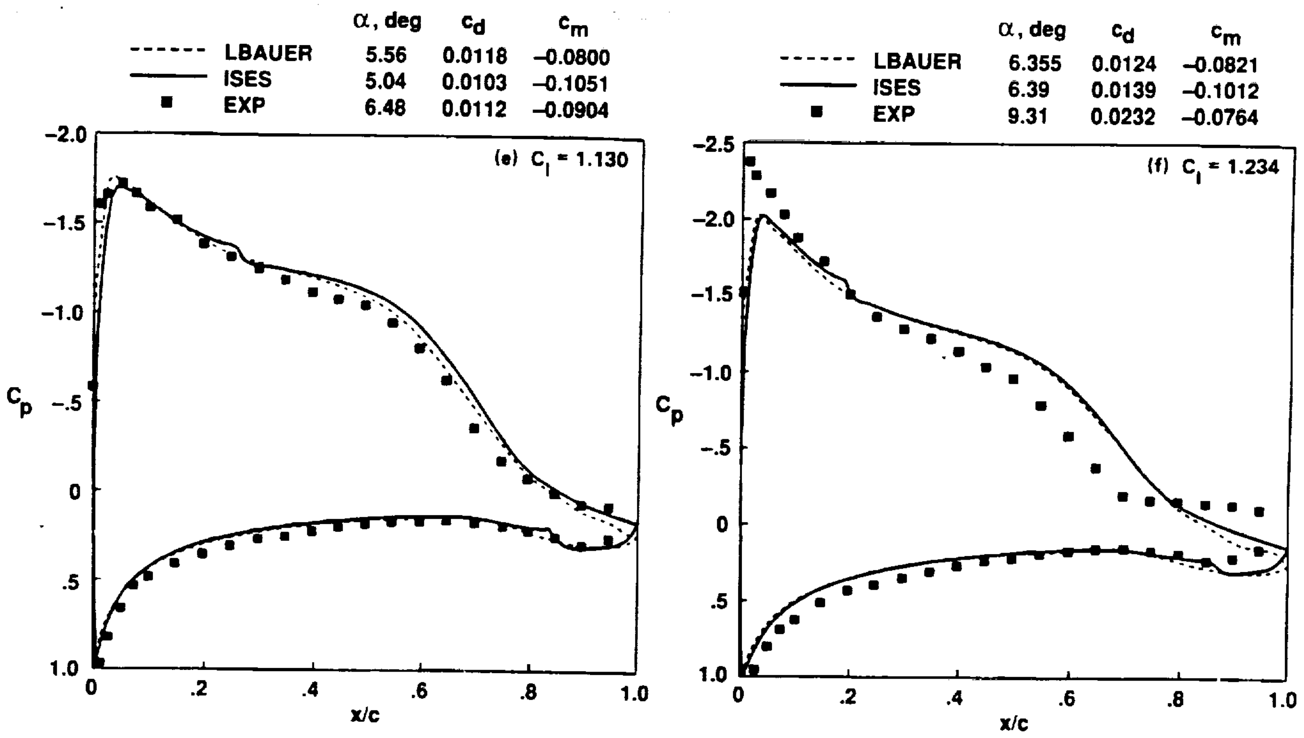

Figure 9. Concluded.

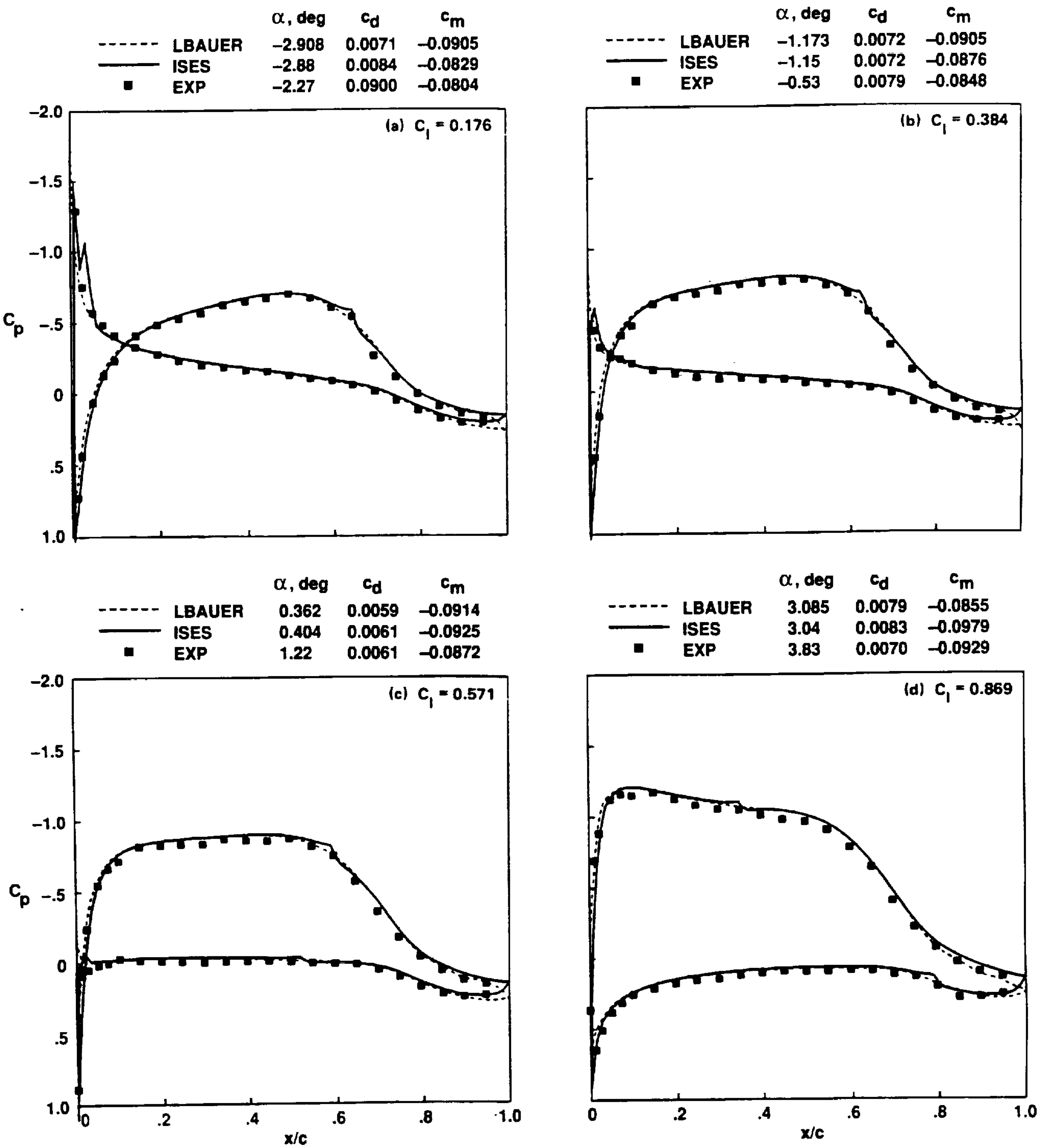

Figure 10. Surface-pressure distributions for LRN 1015 airfoil: M = 0.20, Re = 1,900,000.

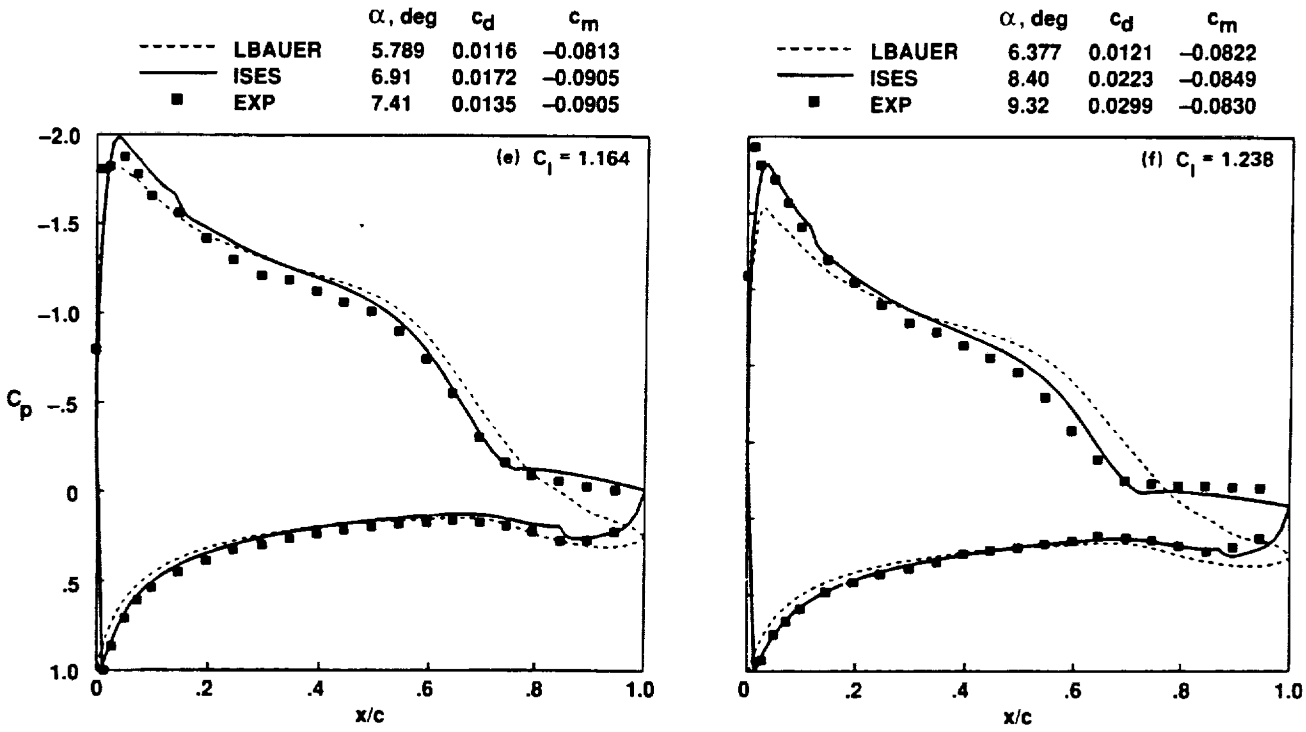

Figure 10. Concluded.

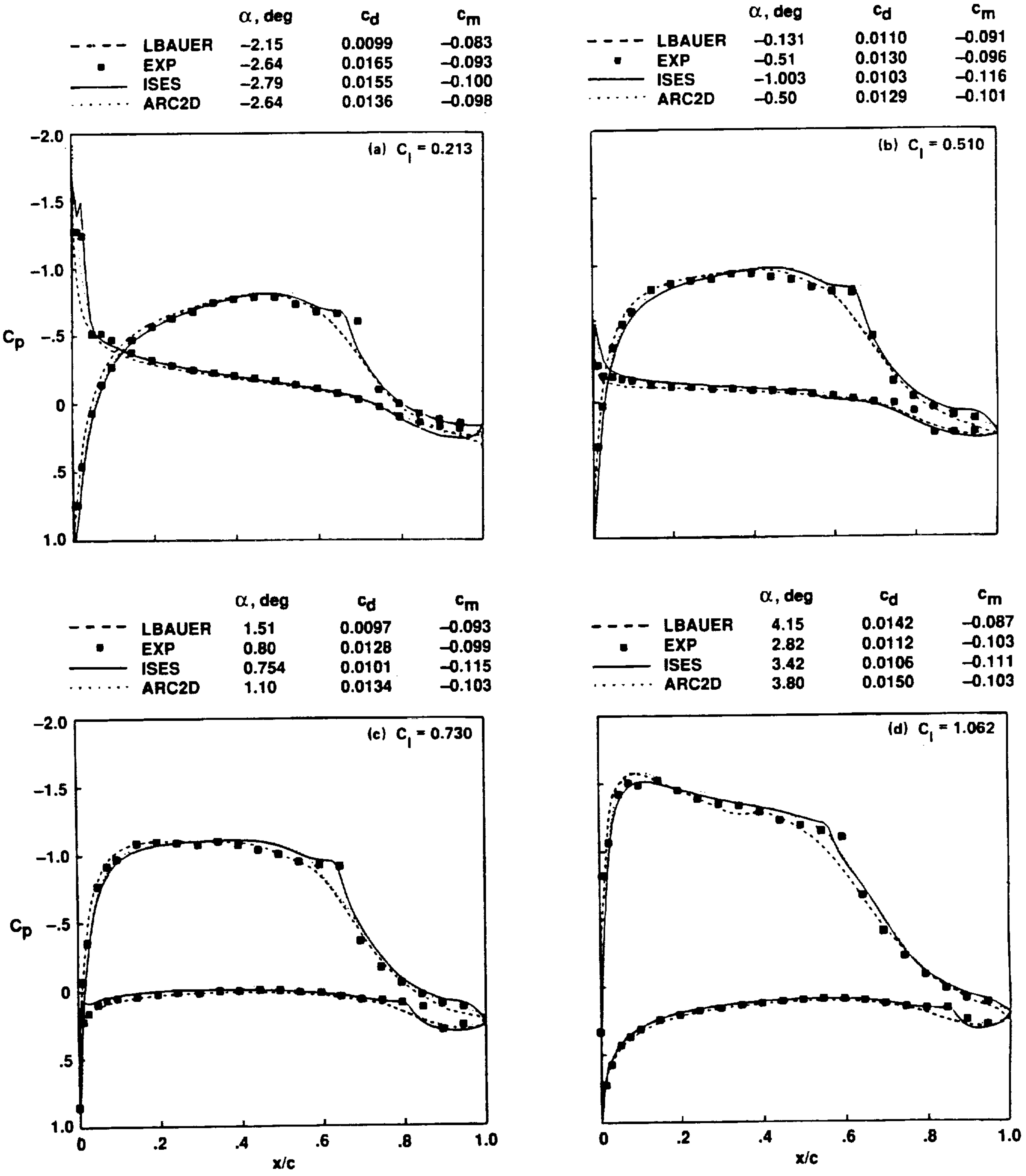

Figure 11. Surface-pressure distributions for LRN 1015 airfoil: M = 0.50, Re = 500,000.

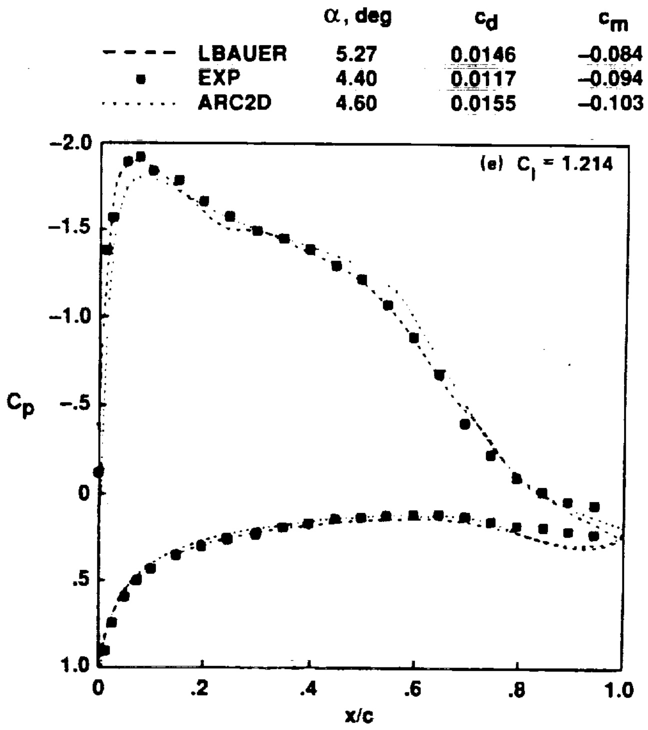

Figure 11. Concluded.

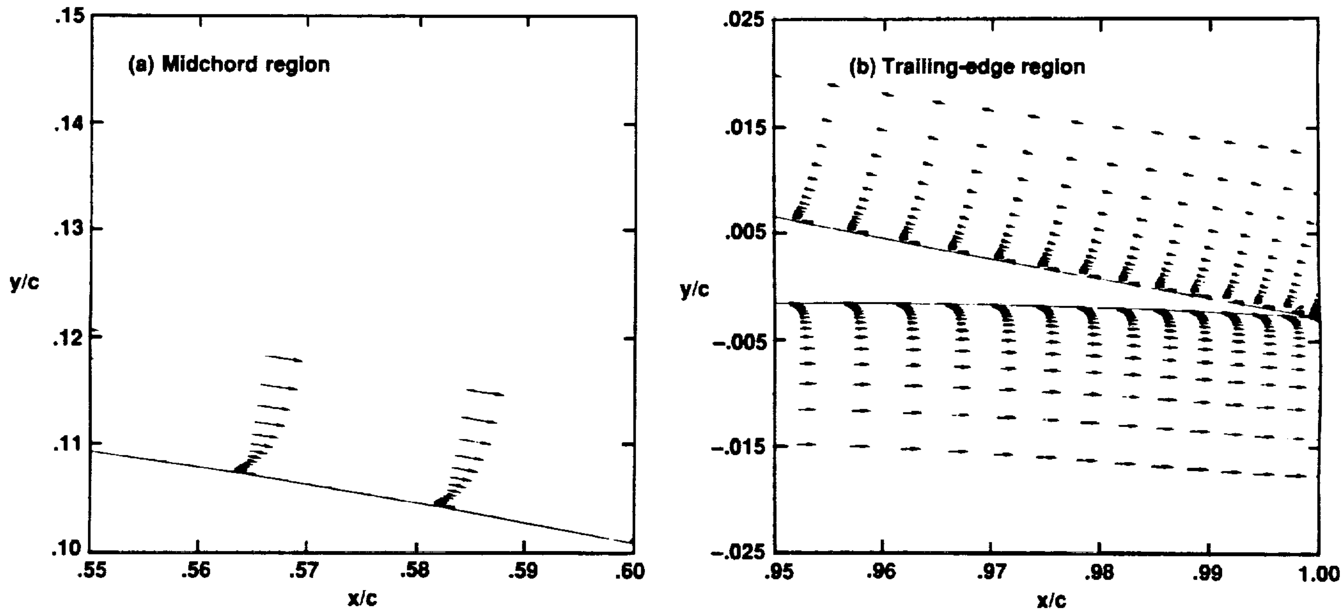

Figure 12. Velocity profiles for LRN 1015 airfoil: M = 0.50, Re = 500,000, c_l = 1.214.

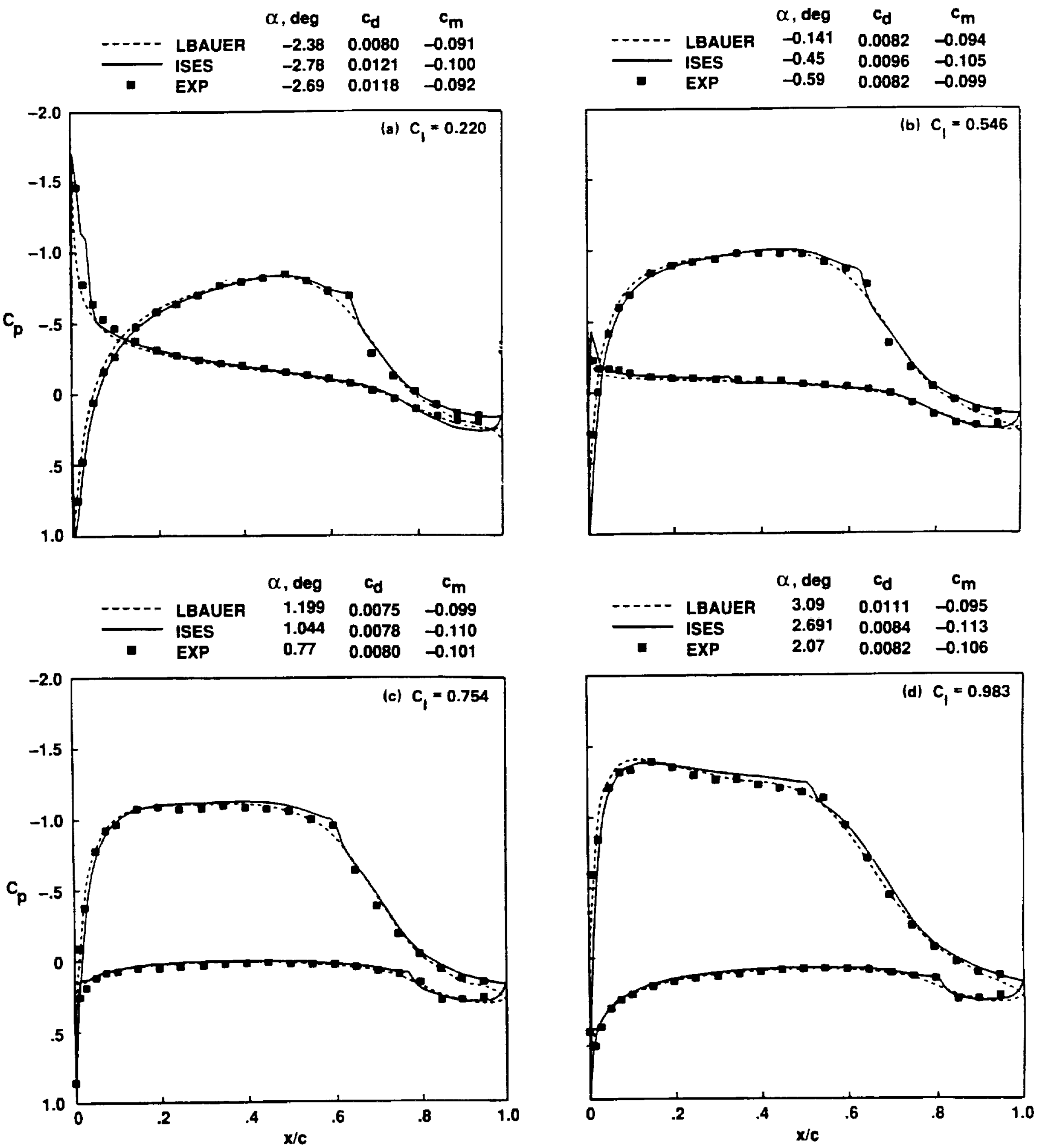

Figure 13. Surface-pressure distributions for LRN 1015 airfoil: M = 0.50, Re = 1,000,000.

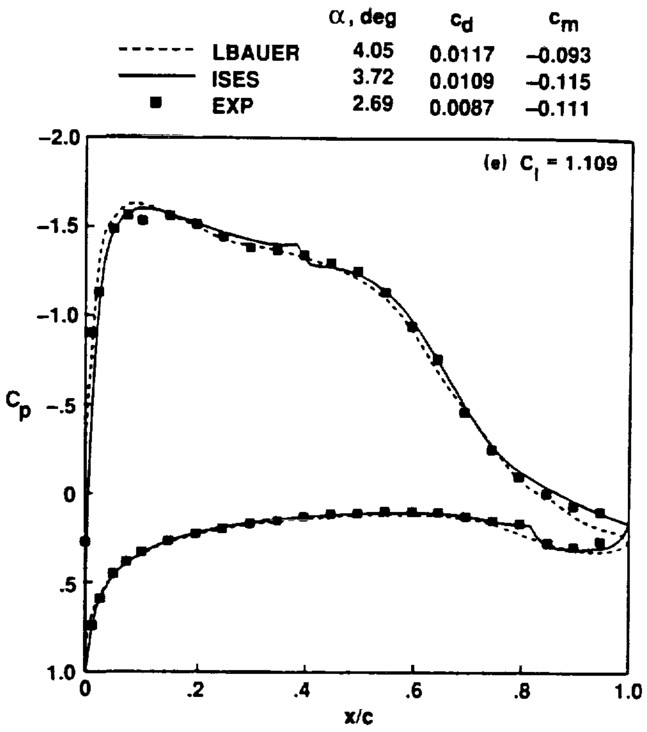

Figure 13. Concluded.

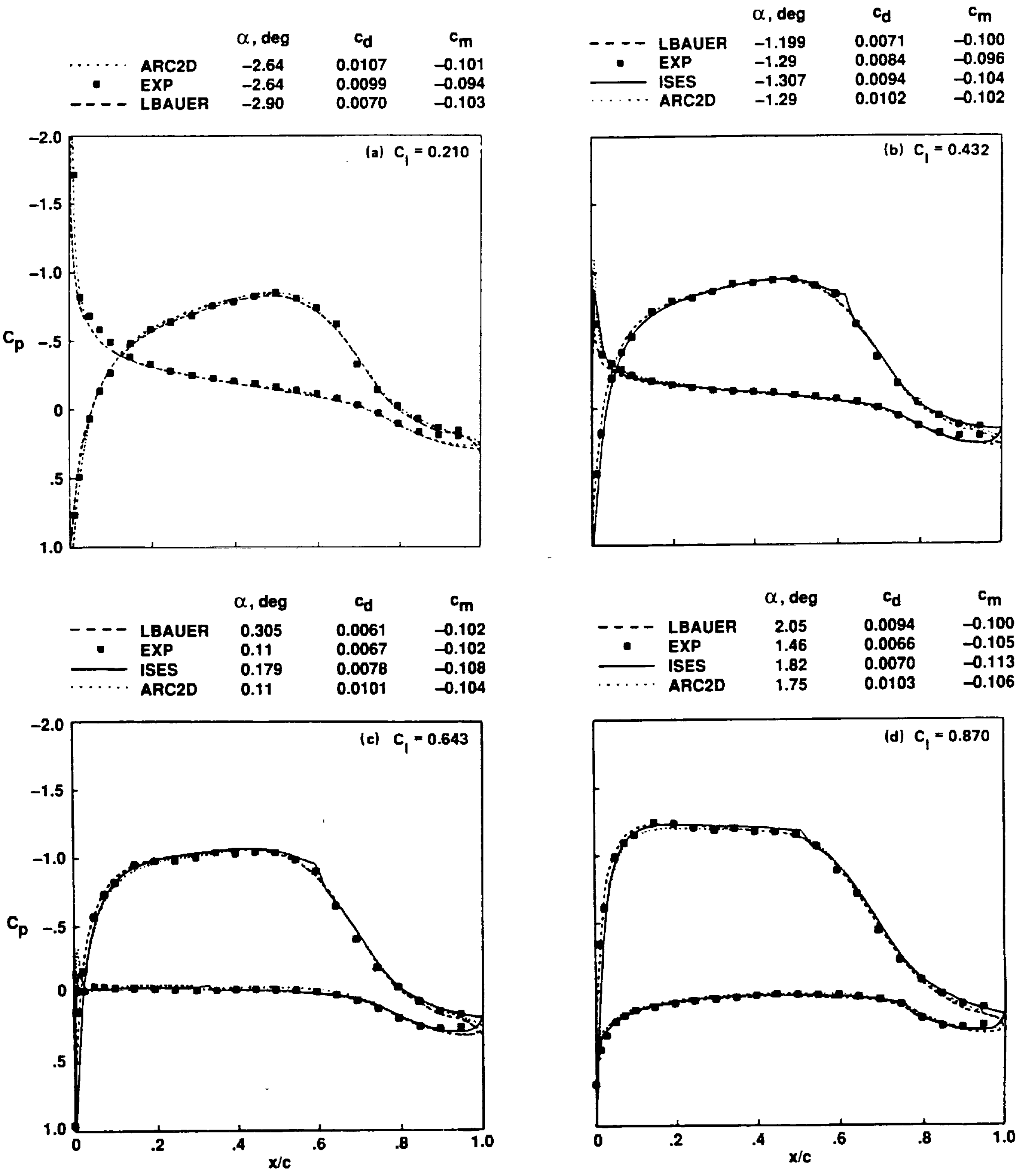

Figure 14. Surface-pressure distributions for LRN 1015 airfoil: M = 0.50, Re = 1,900,000.

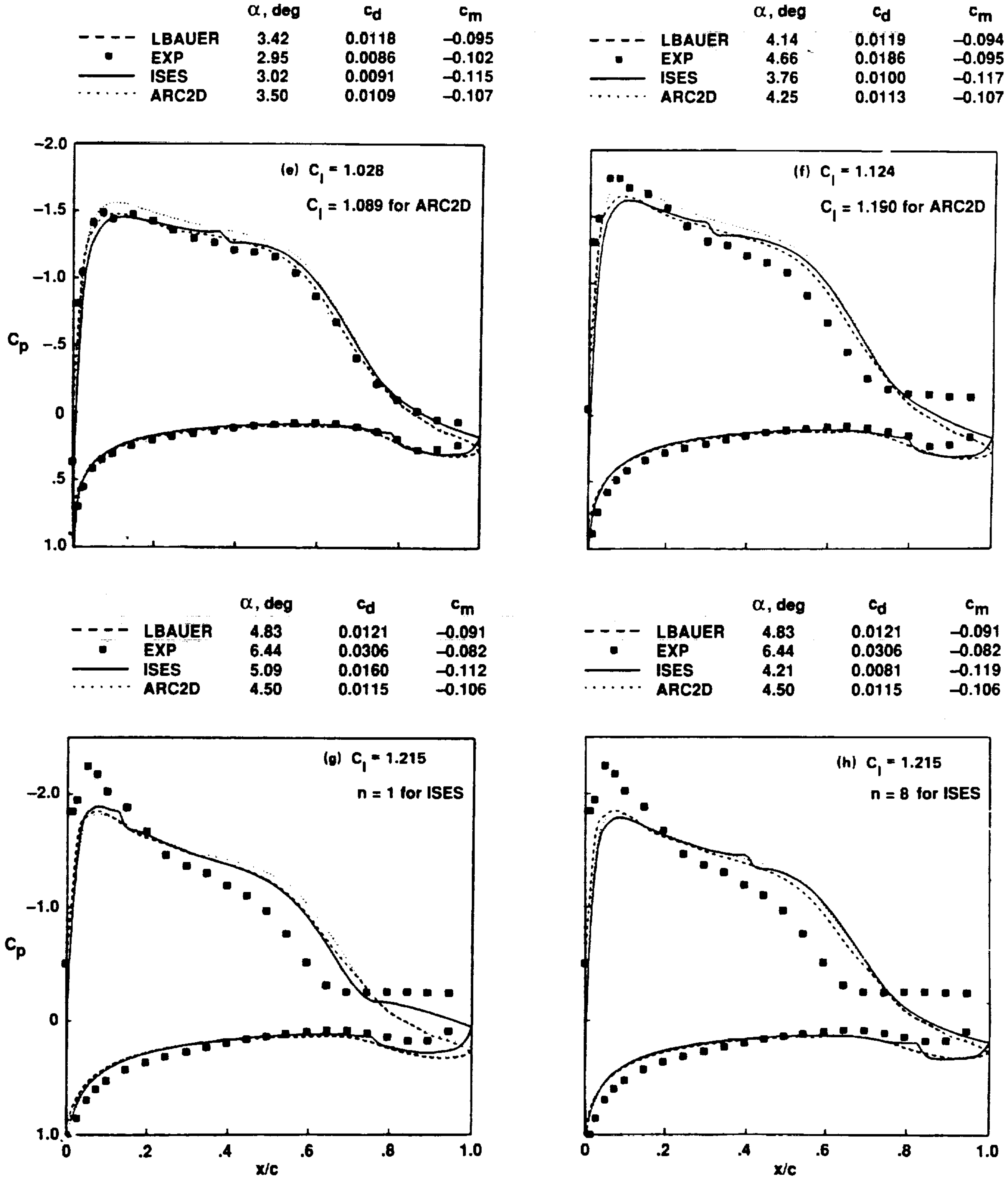

Figure 14. Concluded.

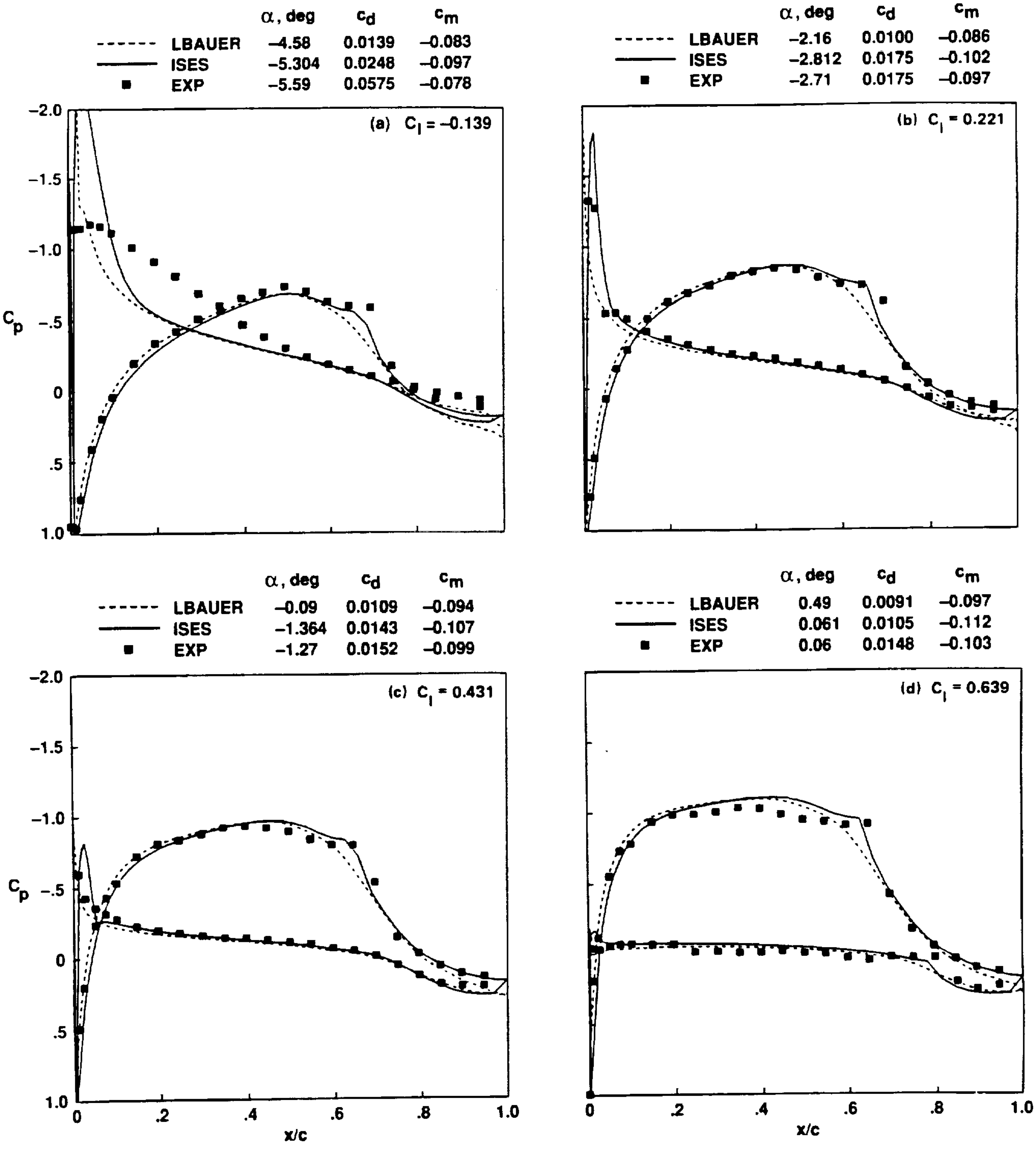

Figure 15. Surface-pressure distributions for LRN 1015 airfoil: M = 0.55, Re = 500,000.

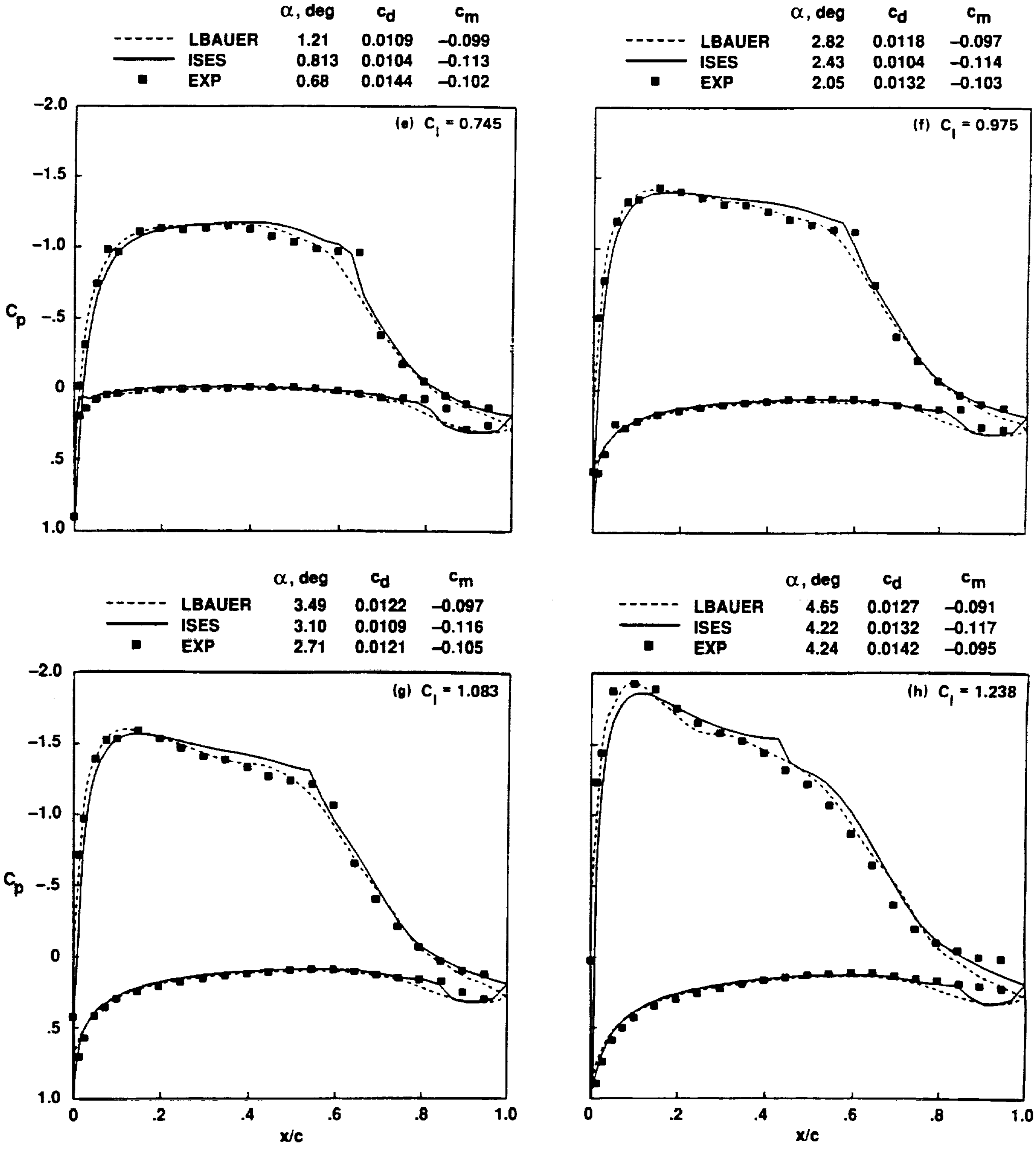

Figure 15. Concluded.

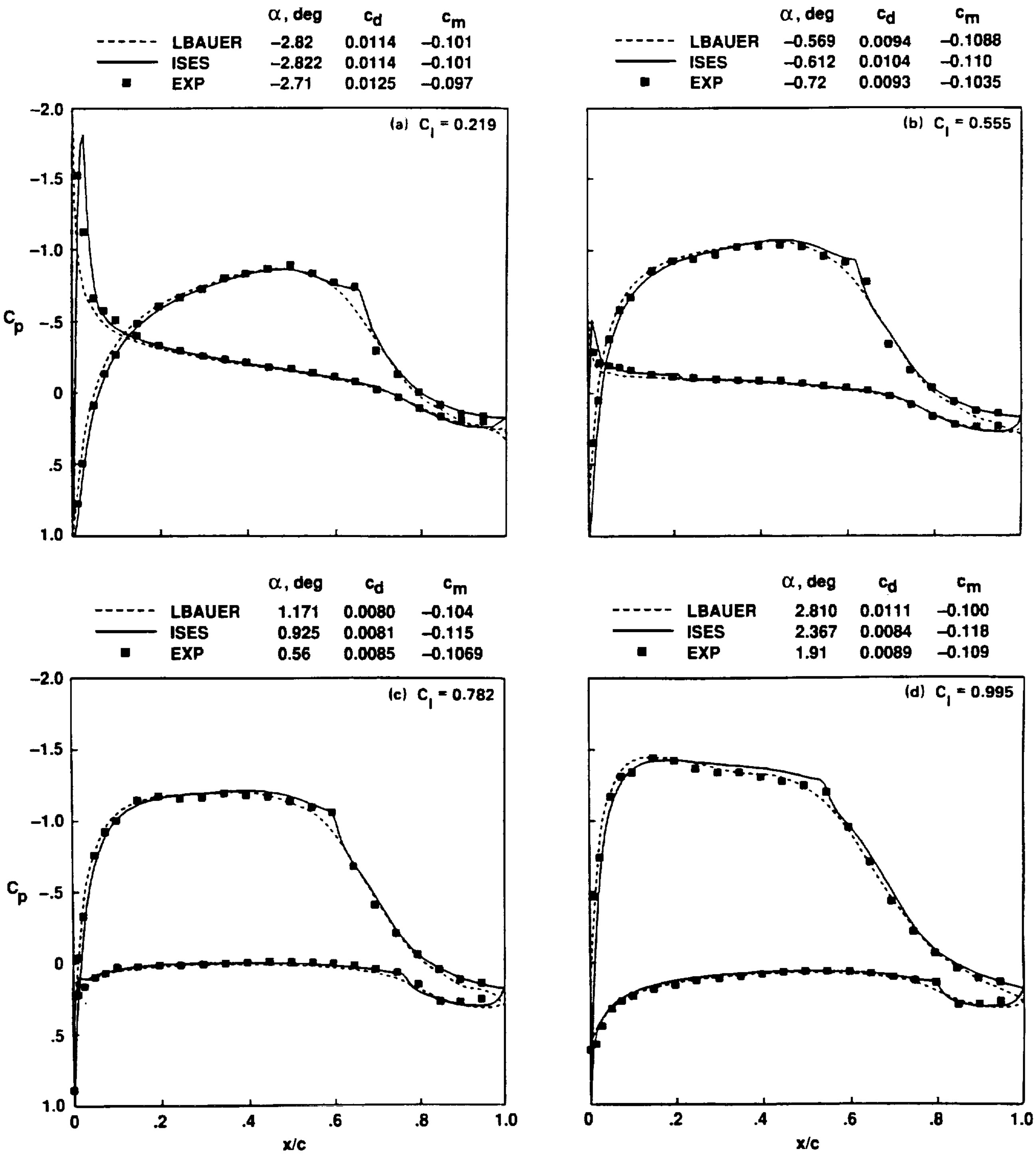

Figure 16. Surface-pressure distributions for LRN 1015 airfoil: M = 0.55, Re = 1,000,000.

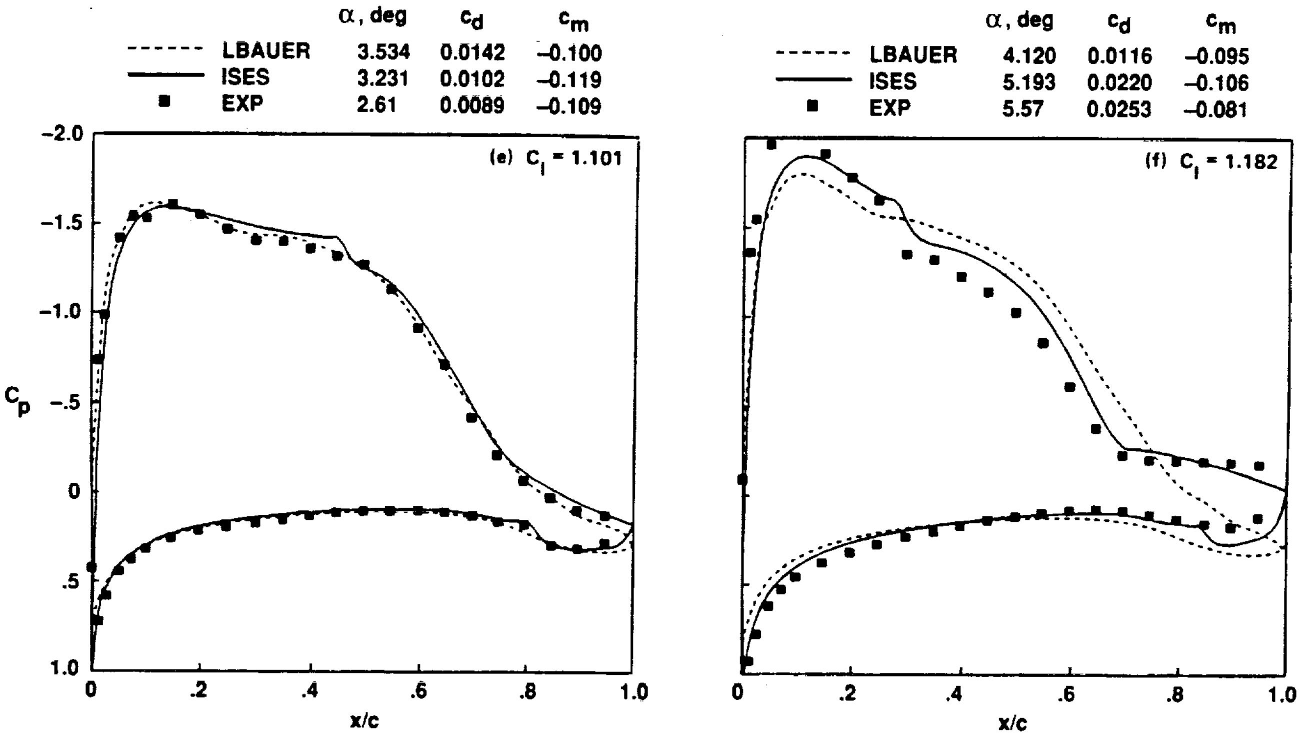

Figure 16. Concluded.

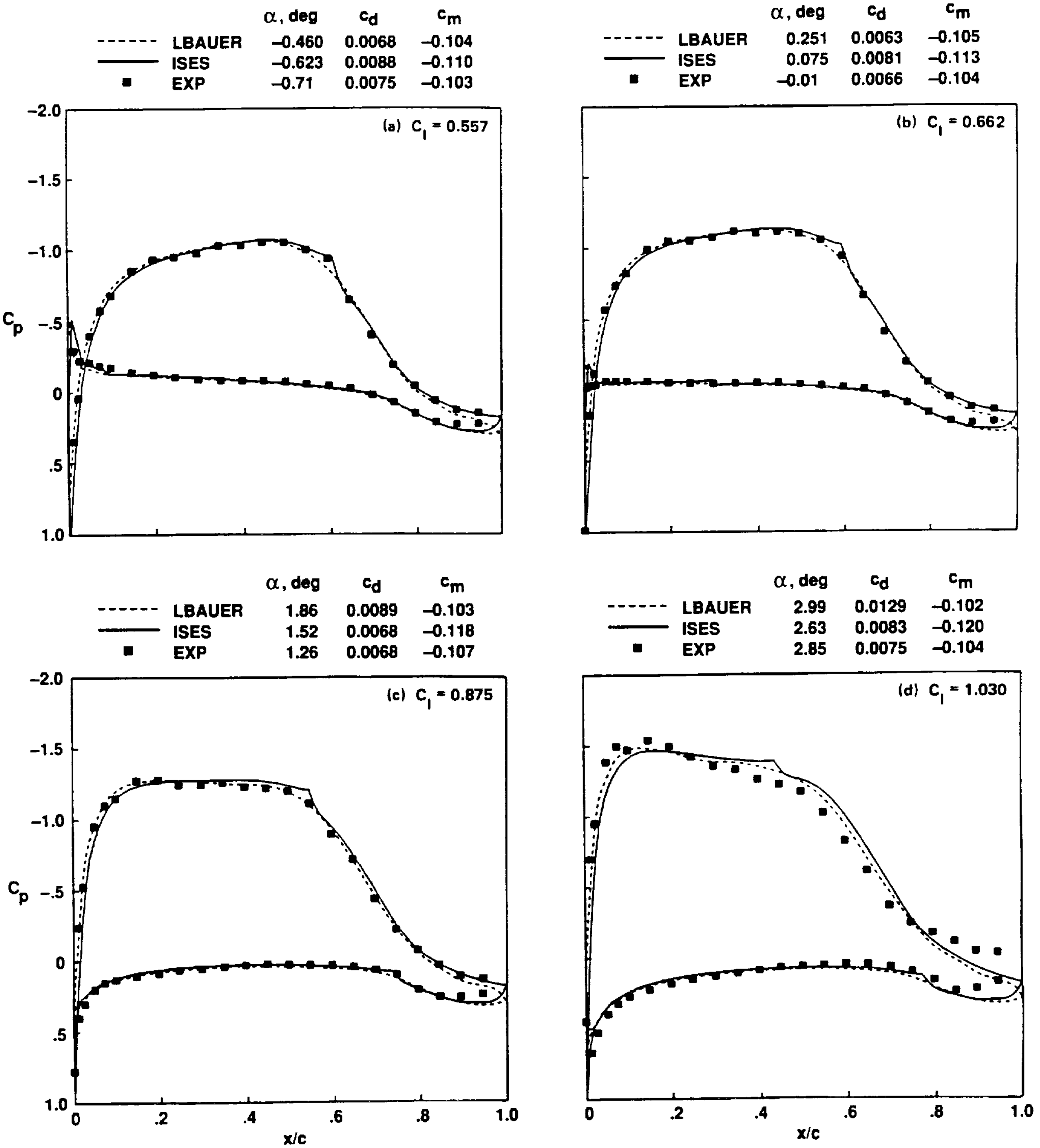

Figure 17. Surface-pressure distributions for LRN 1015 airfoil: M = 0.55, Re = 2,000,000.

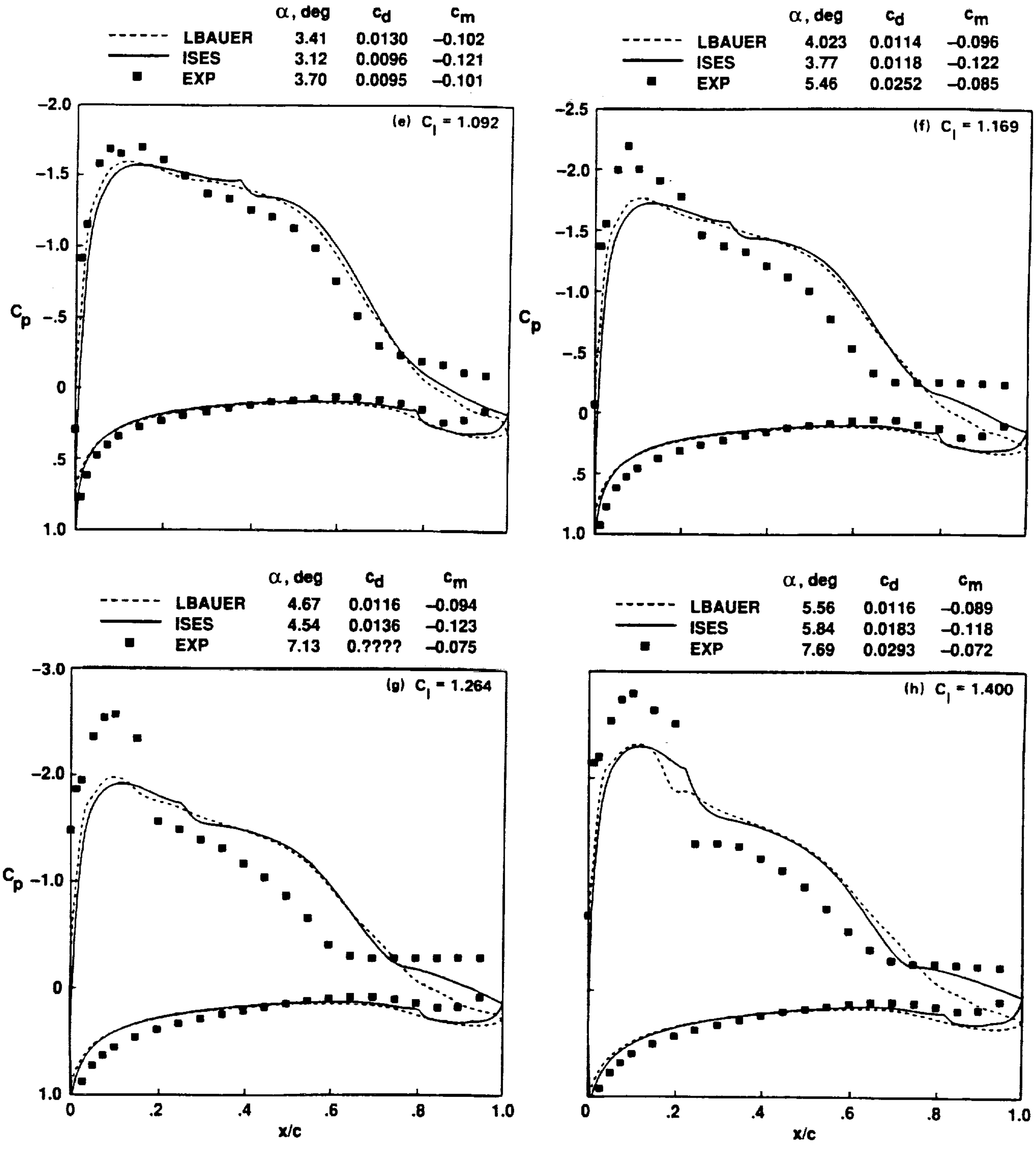

Figure 17. Concluded.

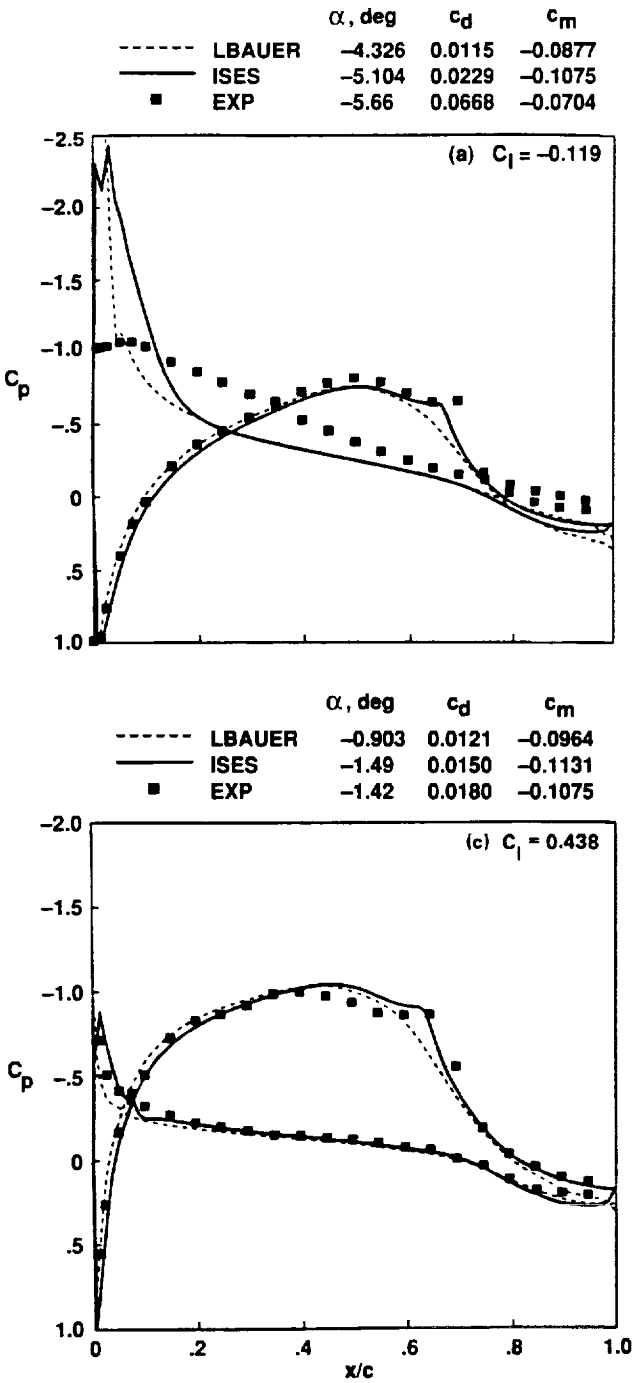

Figure 18. Surface-pressure distributions for LRN 1015 airfoil: M = 0.60, Re = 500,000.

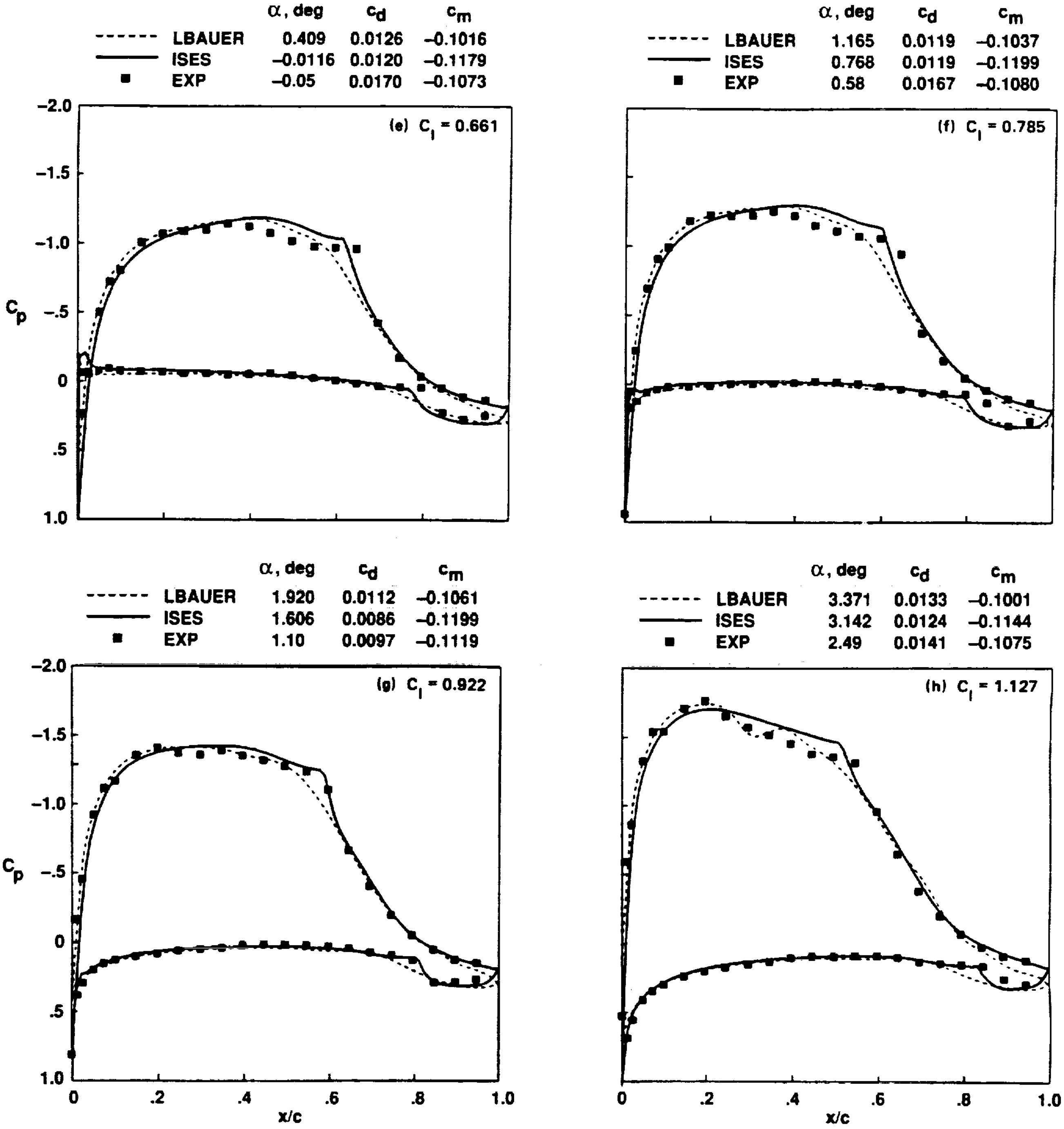

Figure 18. Continued.

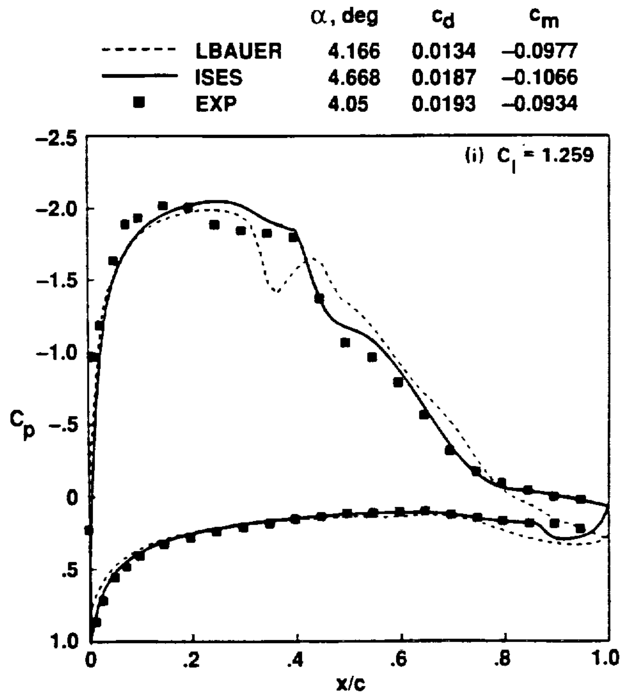

Figure 18. Concluded.

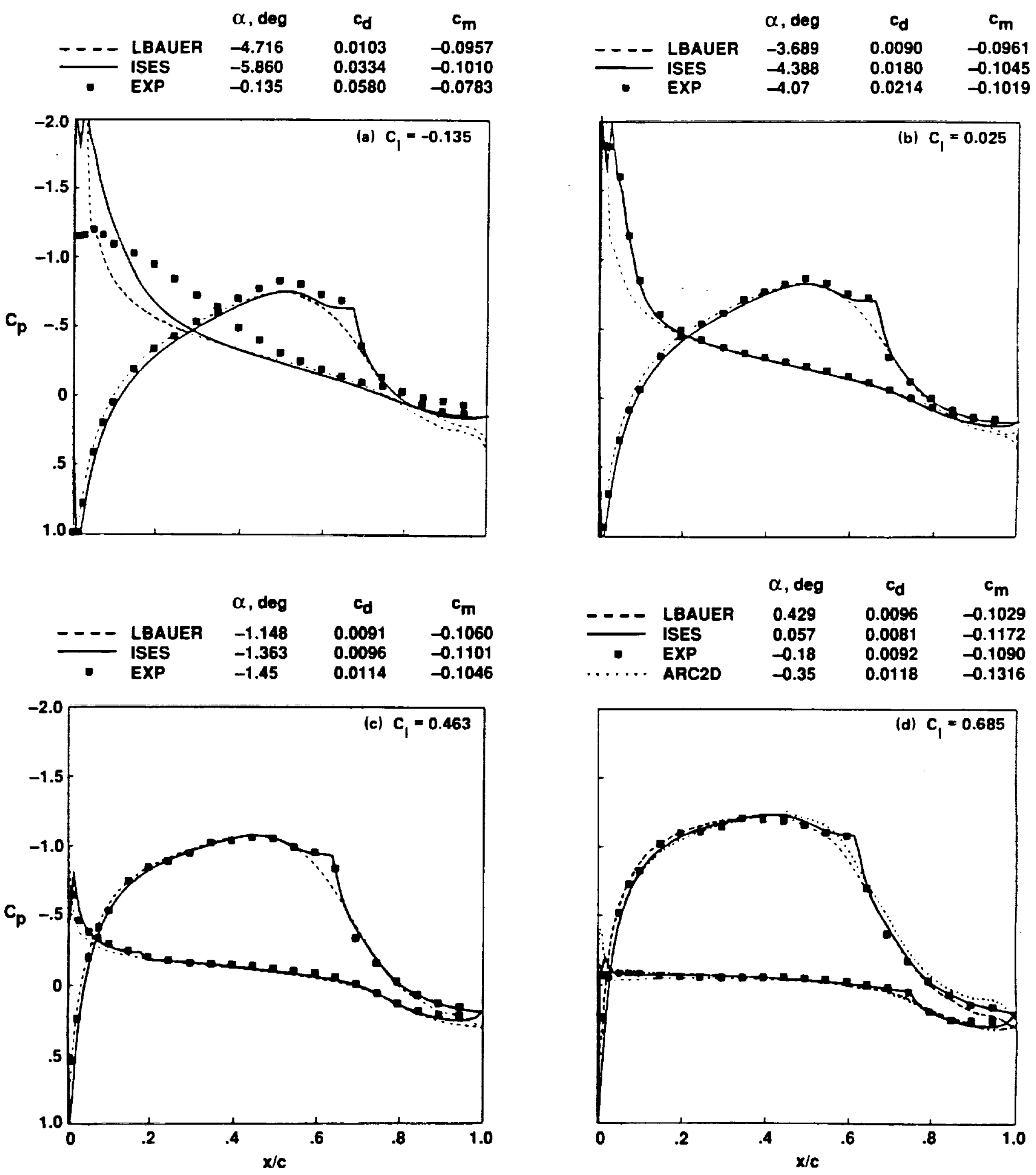

Figure 19. Surface-pressure distributions for LRN 1015 airfoil: M = 0.60, Re = 1,000,000.

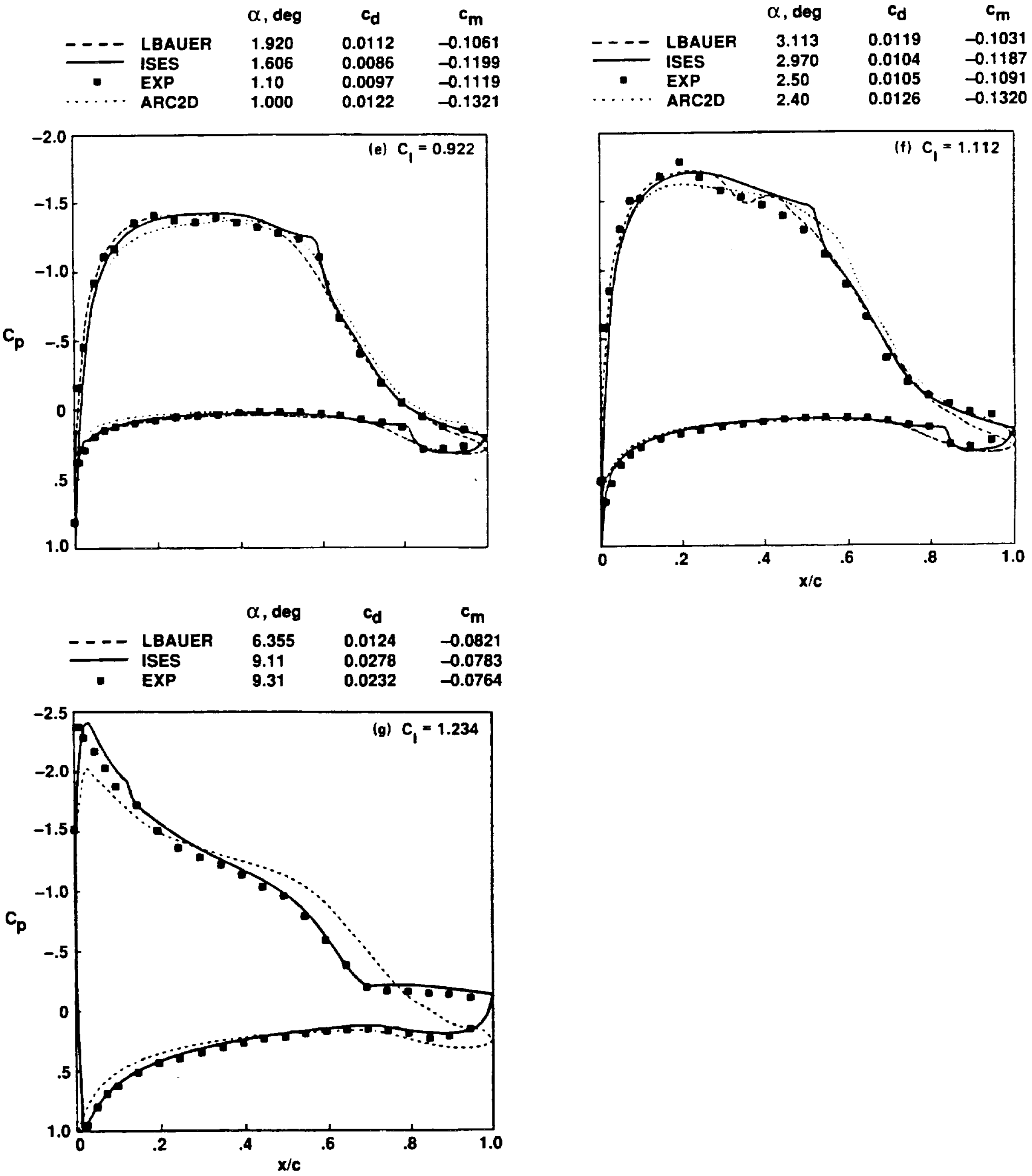

Figure 19. Concluded.

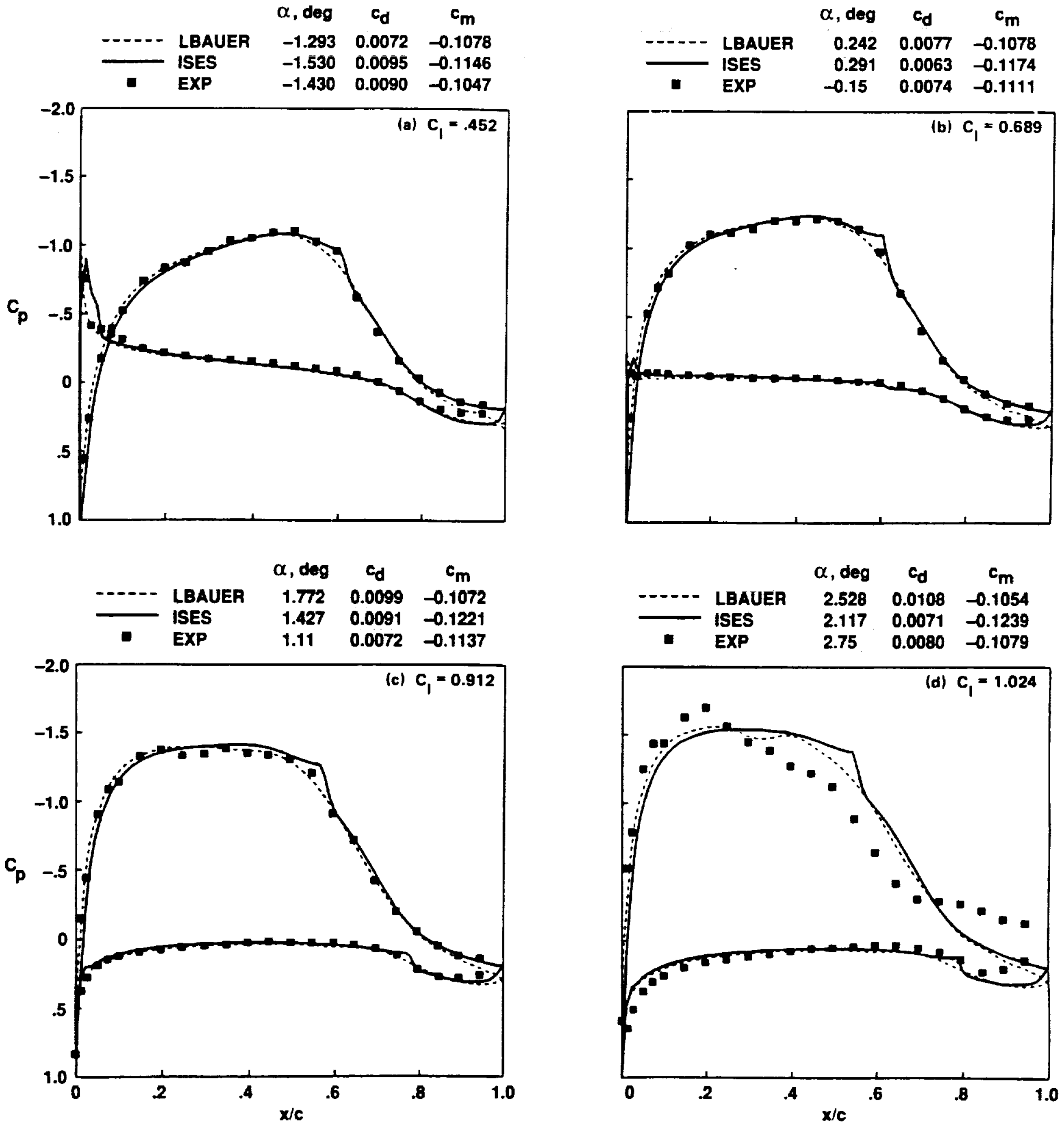

Figure 20. Surface-pressure distributions for LRN 1015 airfoil: M = 0.60, Re = 2,000,000.

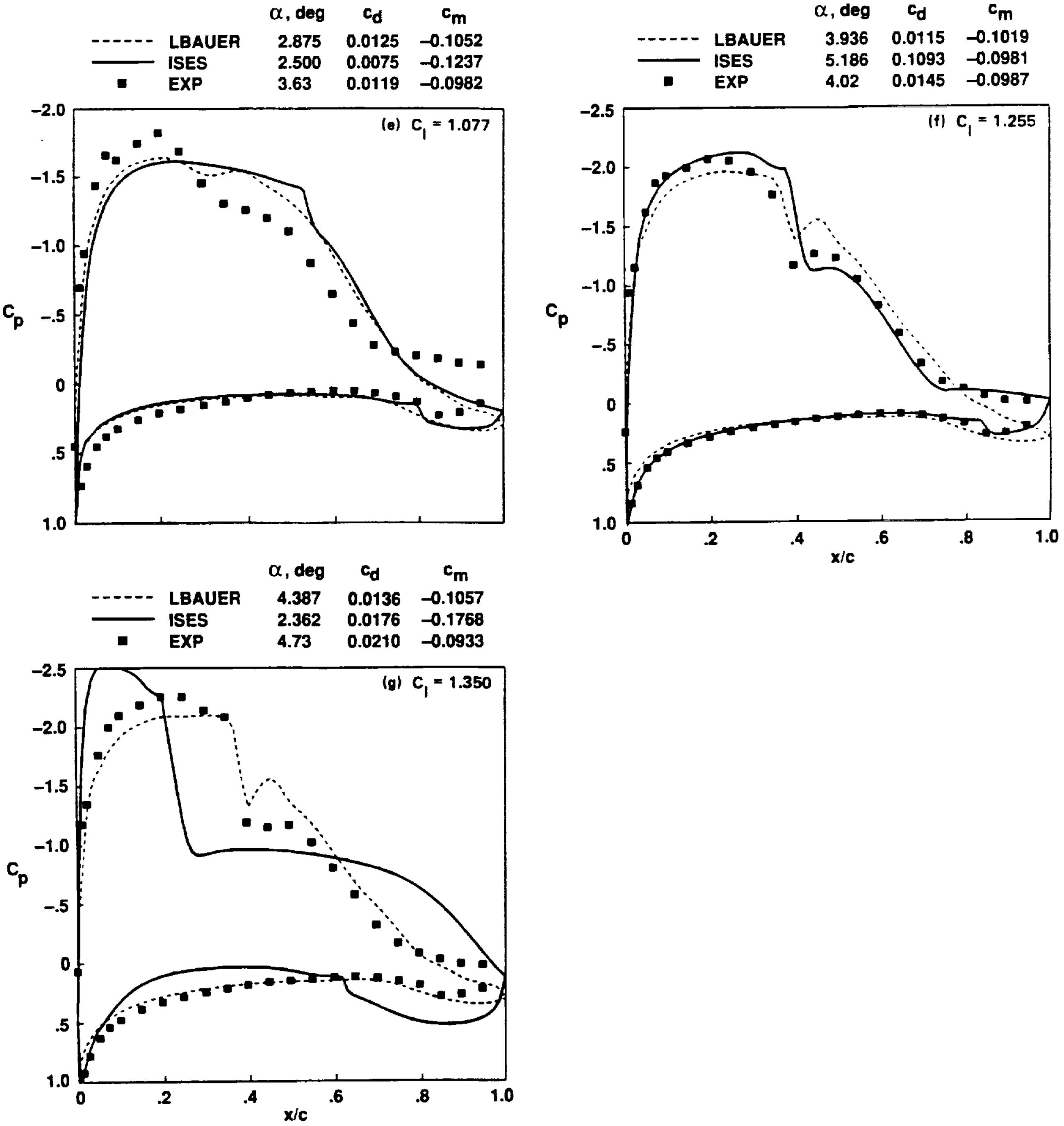

Figure 20. Concluded.

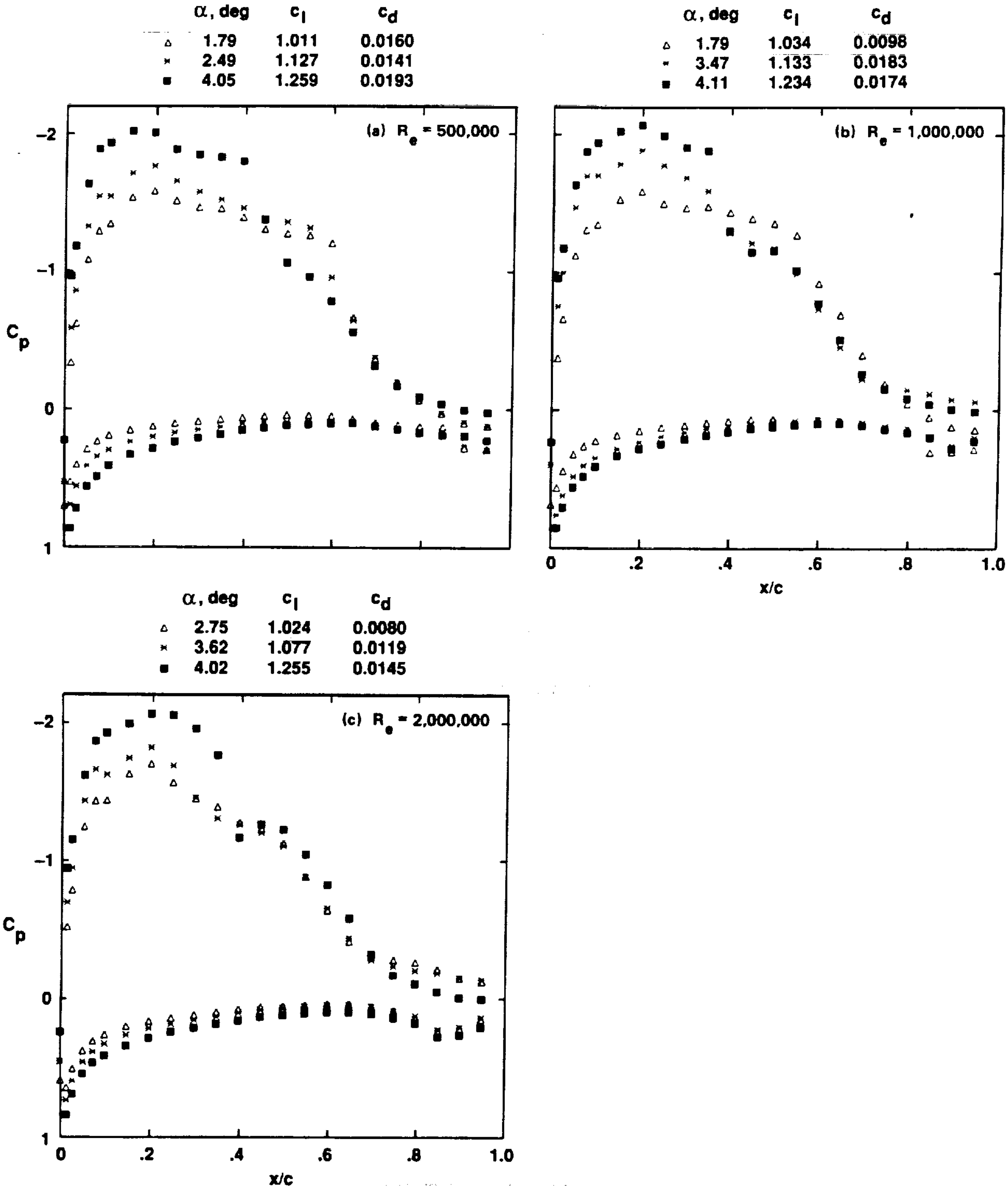

Figure 21. Experimental surface-pressure distributions near stall for LRN 1015 airfoil: M = 0.60.

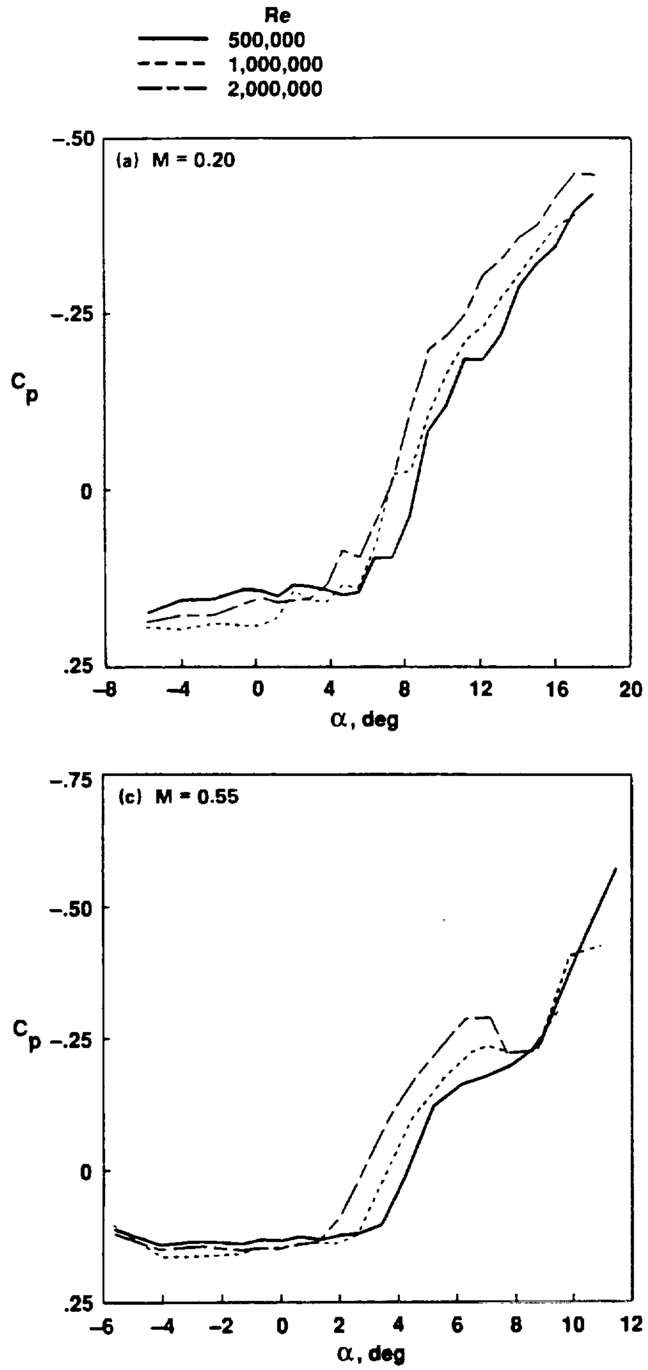

Figure 22. Upper-surface pressure coefficients for LRN 1015 airfoil: x/c = 0.95.

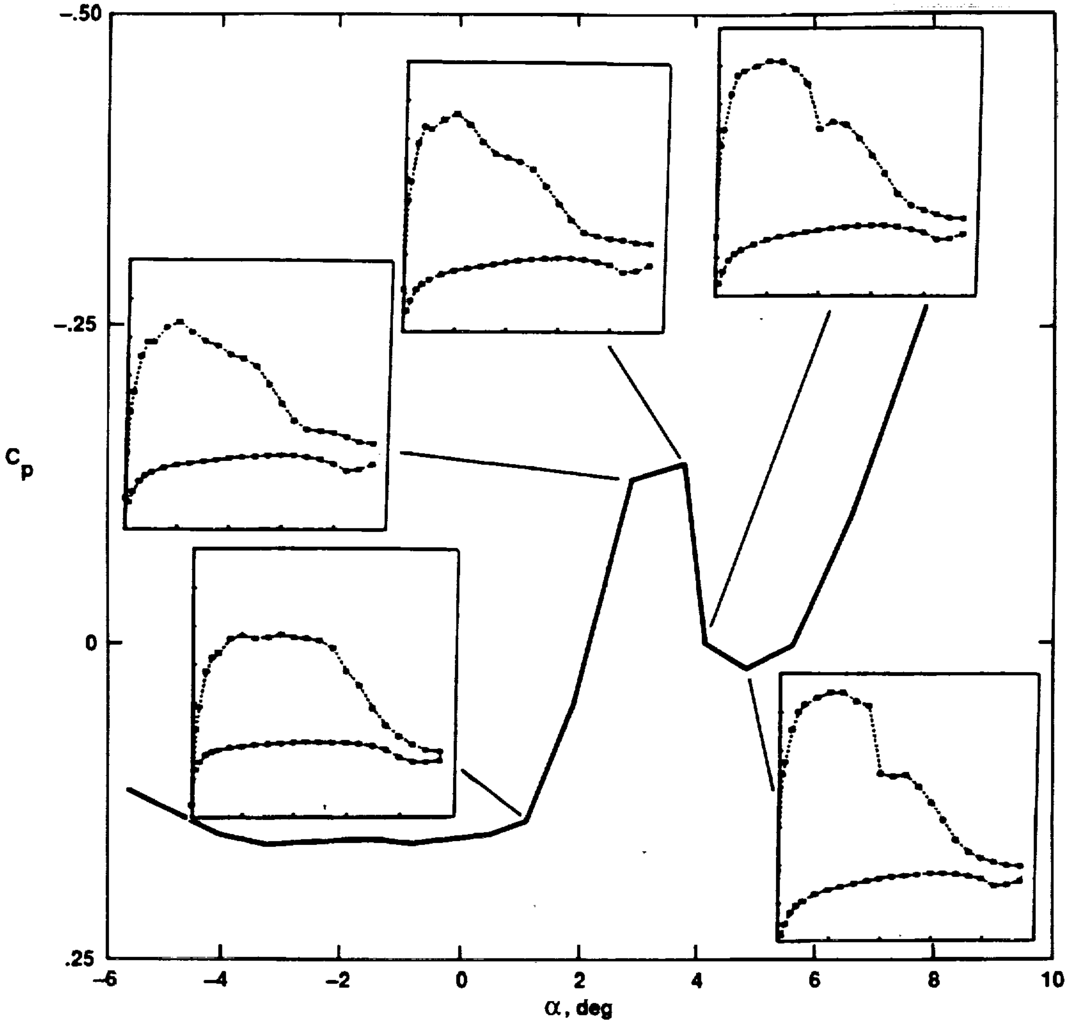

Figure 23. Experimental upper-surface pressure coefficients with selected surface-pressure distributions for LRN 1015 airfoil: x/c = 0.95, M = 0.60, Re = 2,000,000.

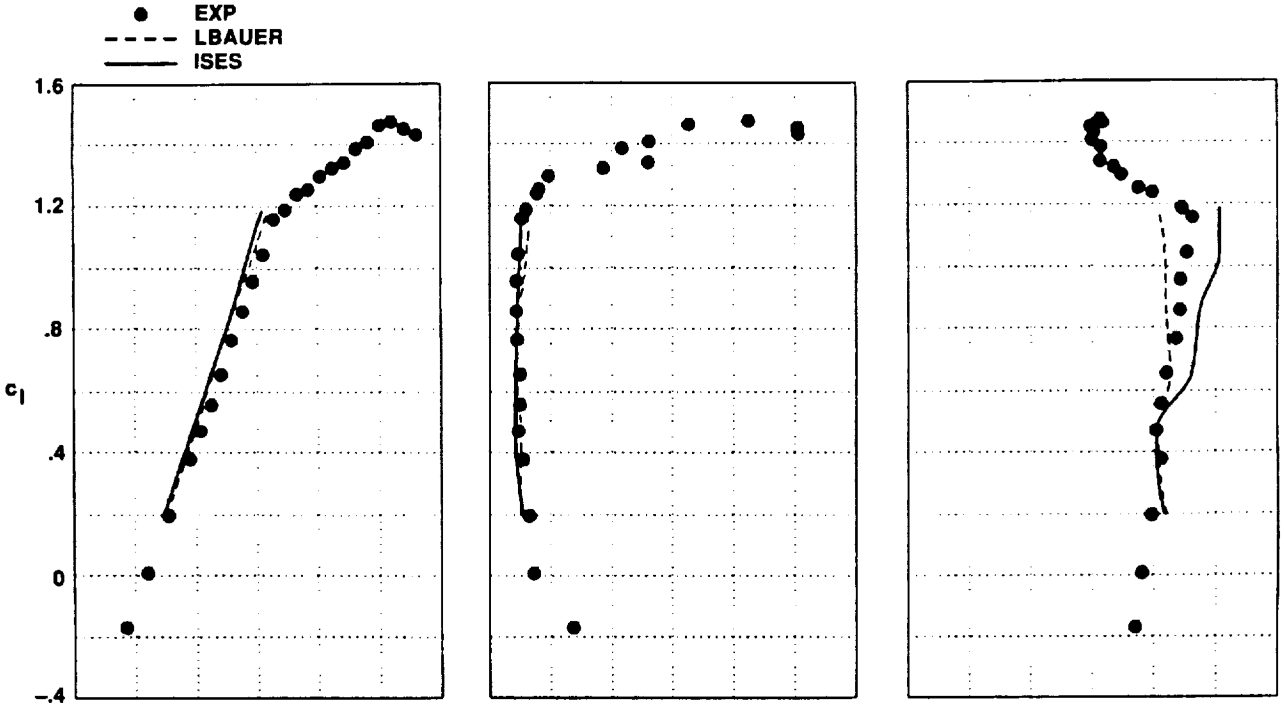

(a) M = 0.20, Re = 500,000

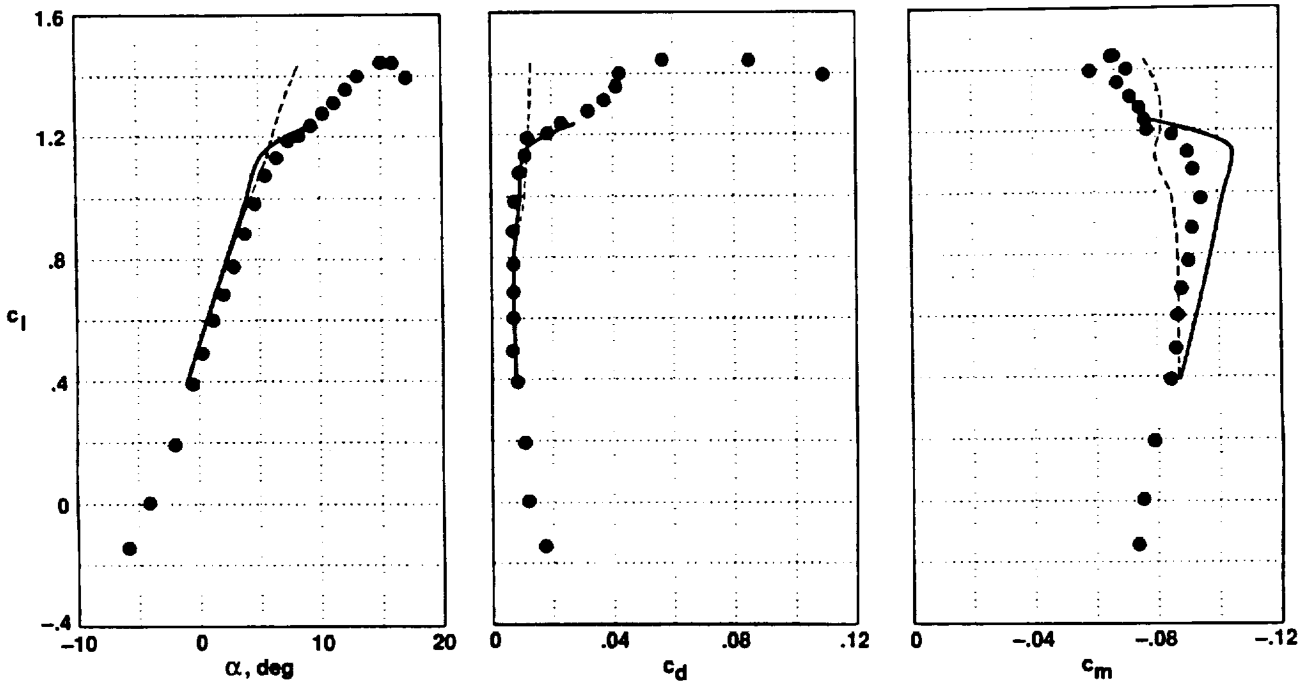

(b) M = .20, Re = 1,000,000

Figure 24. Aerodynamic force and moment coefficients for LRN 1015 airfoil.

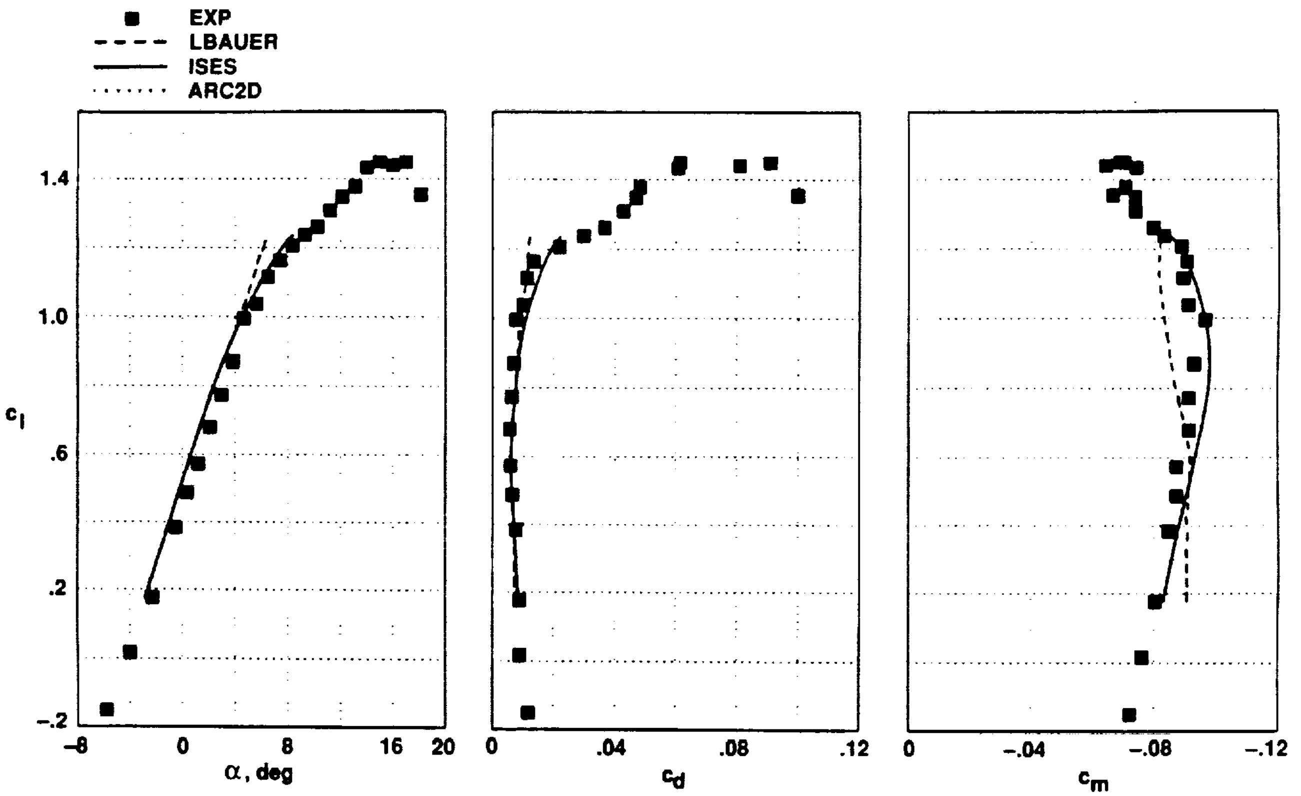

(c) M = .20, Re = 1,900,000

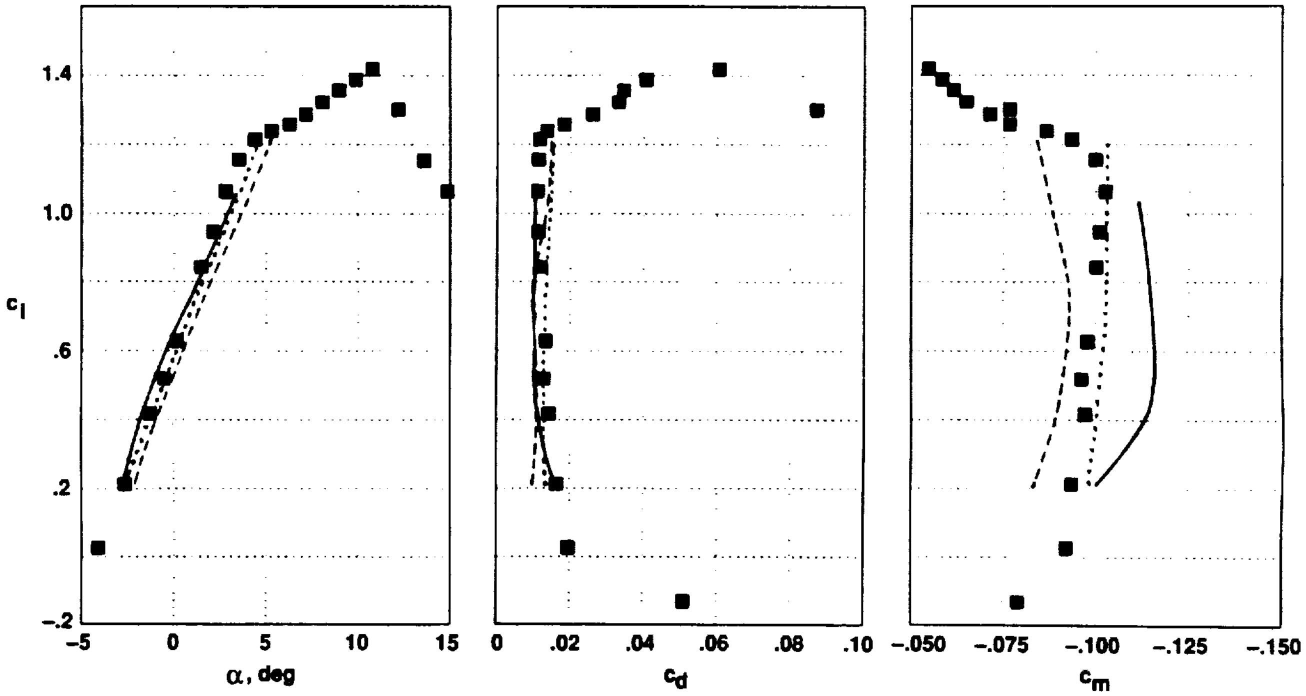

(d) M = .50, Re = 500,000

Figure 24. Continued.

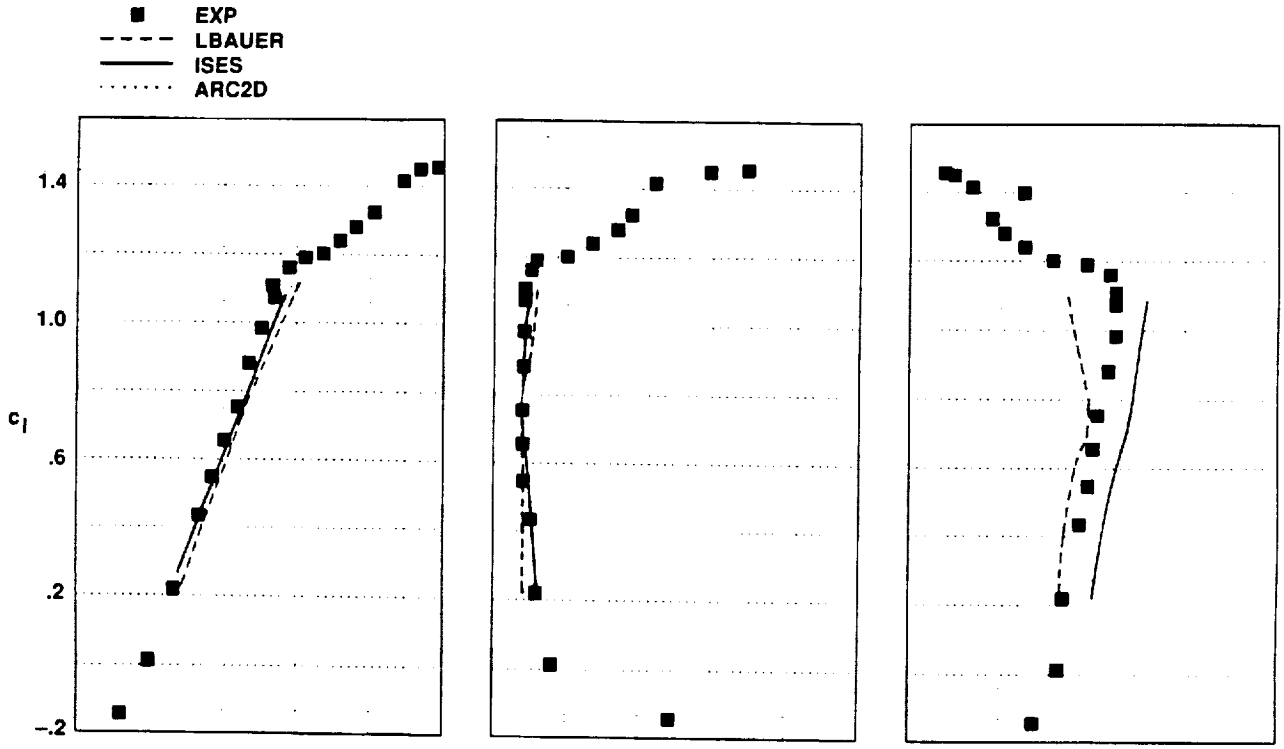

(e) M = 0.50, Re = 1,000,000

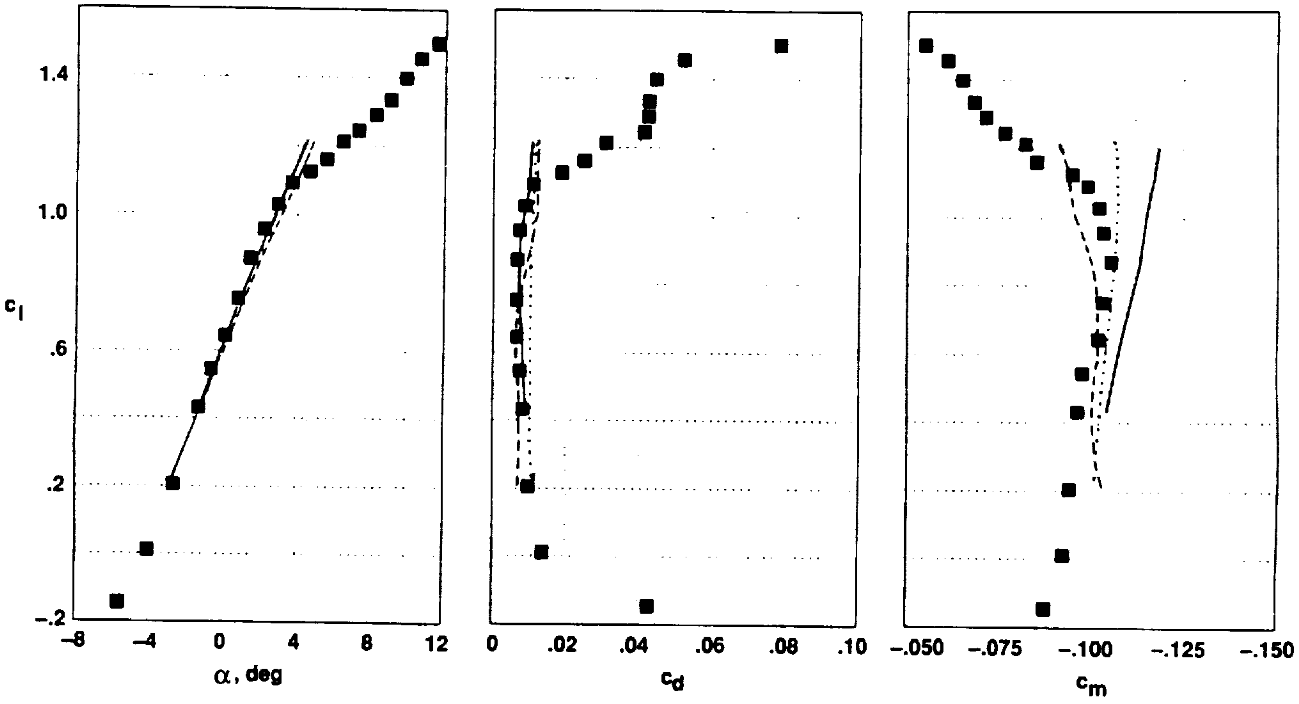

(f) M = 0.50, Re = 2,000,000

Figure 24. Continued.

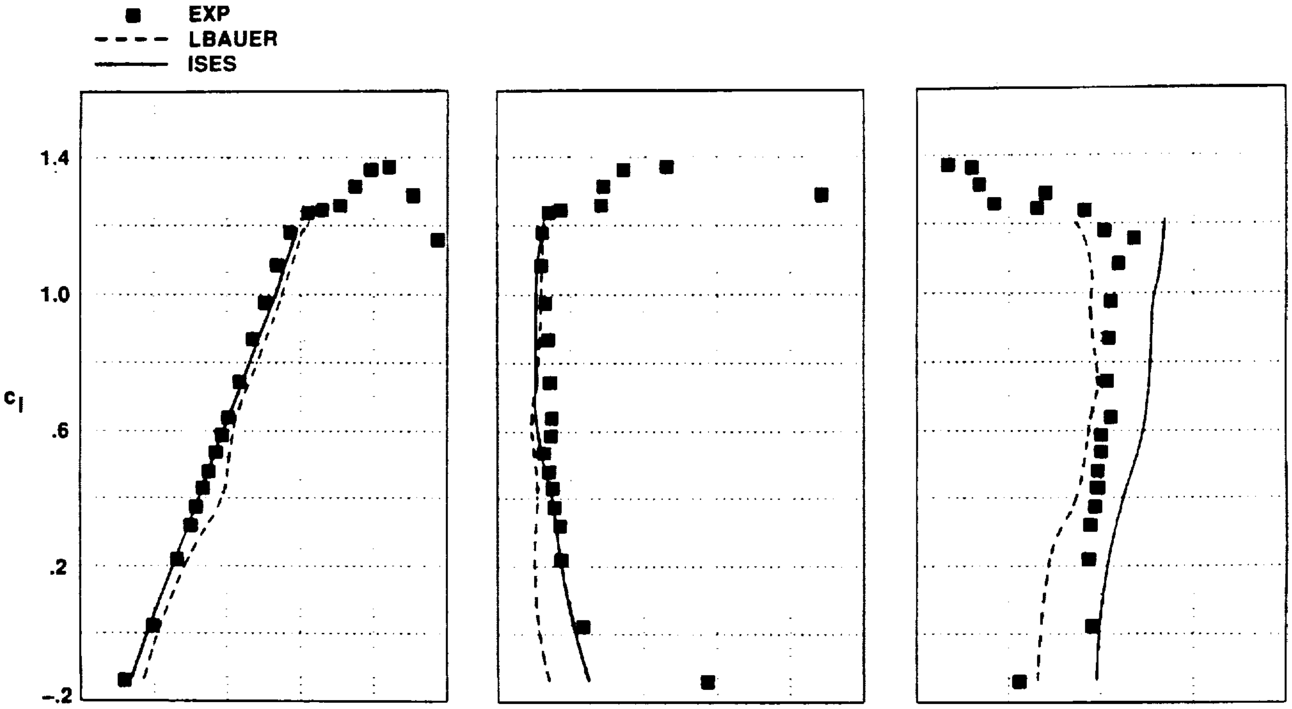

(g) M = 0.55, Re = 500,000

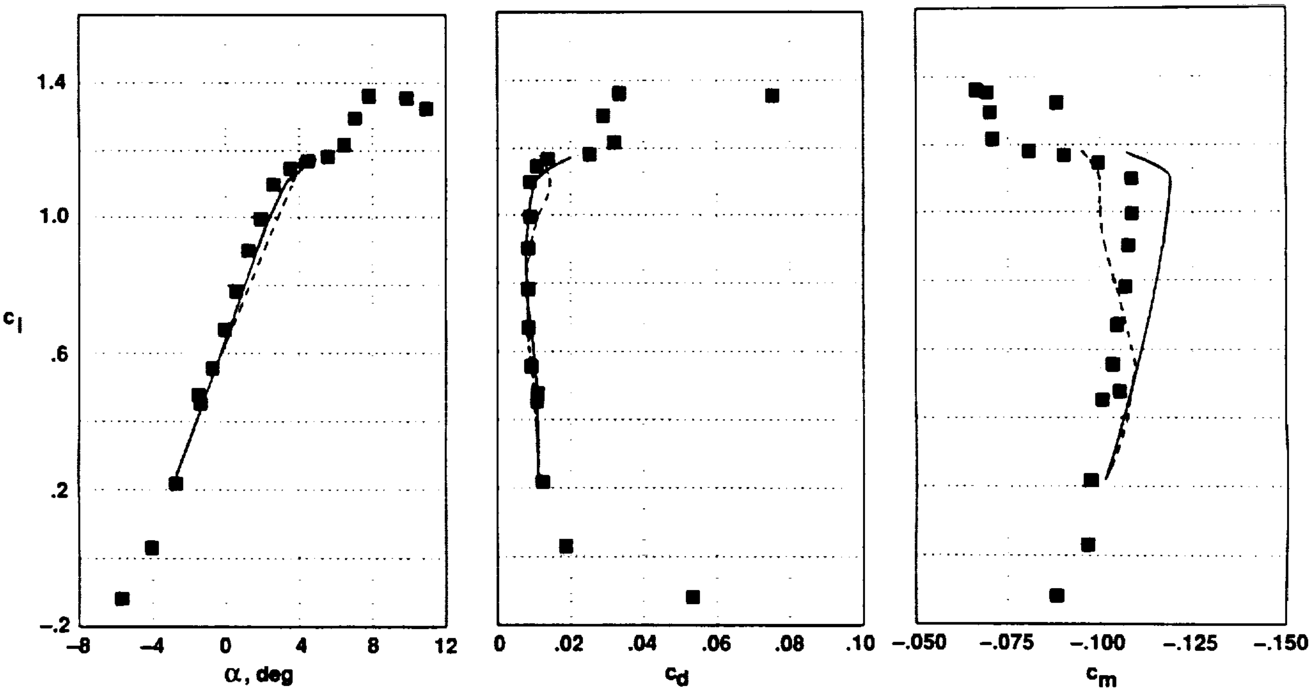

(h) M = 0.55, Re = 1,000,000

Figure 24. Continued.

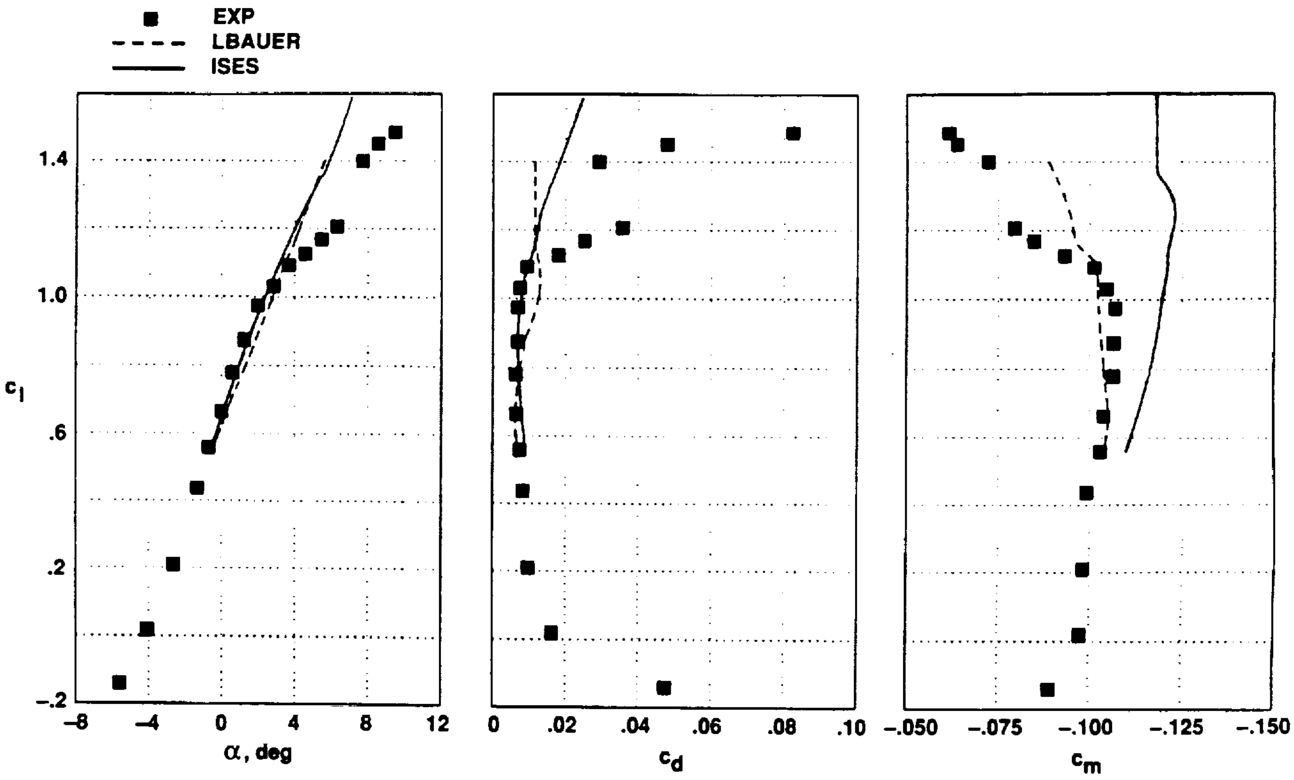

(i) M = 0.55, Re = 2,000,000

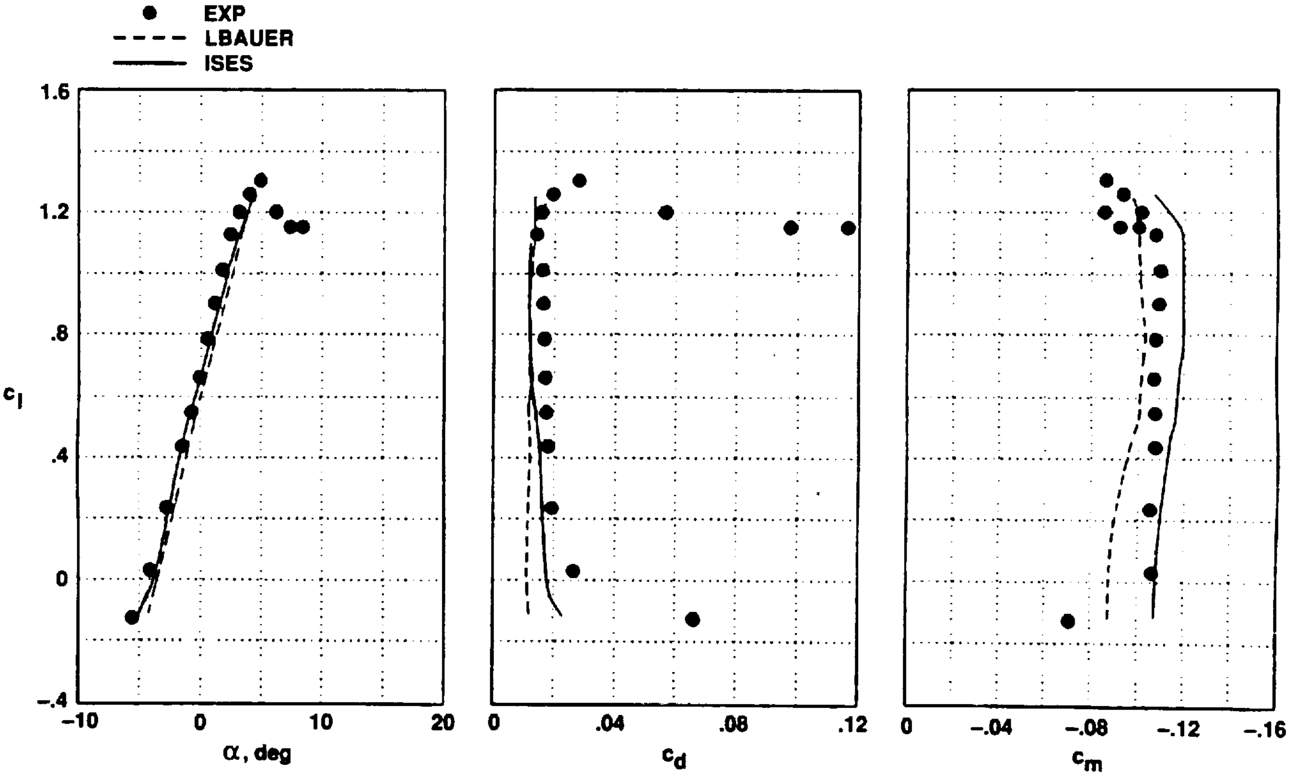

(j) M = 0.60, Re = 500,000

Figure 24. Continued.

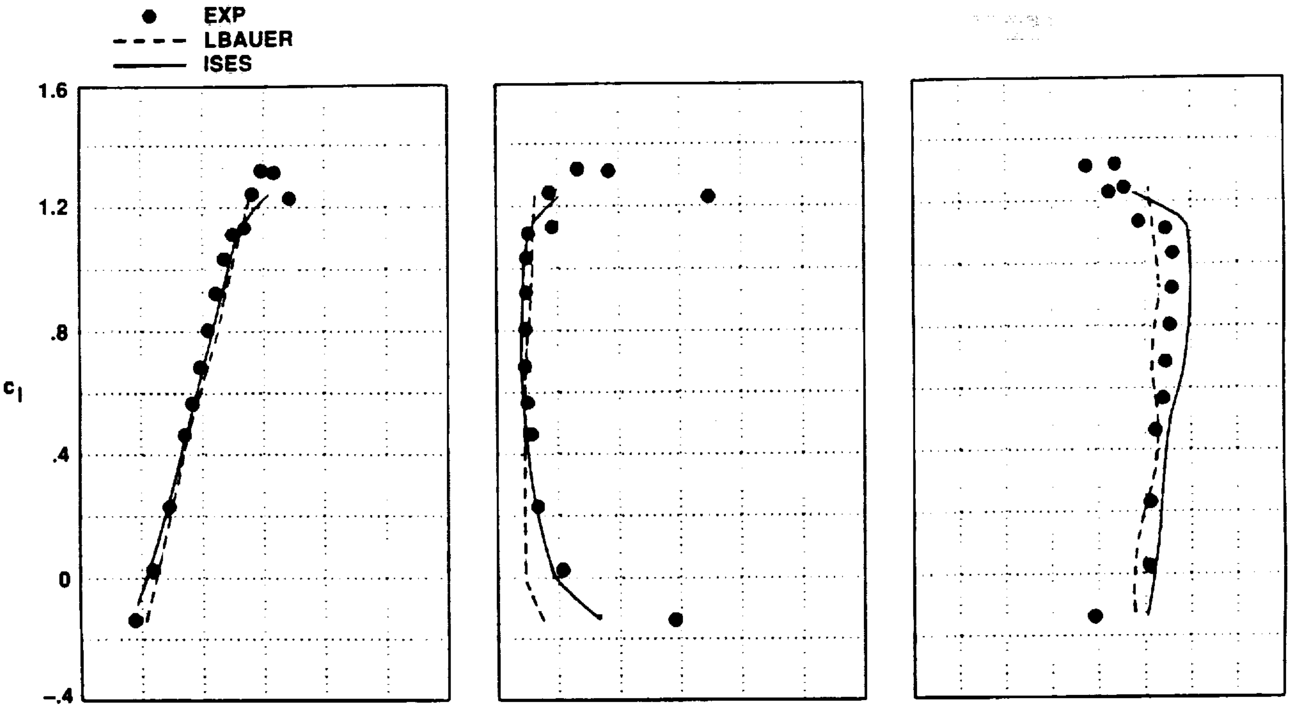

(k) M = 0.60, Re = 1,000,000

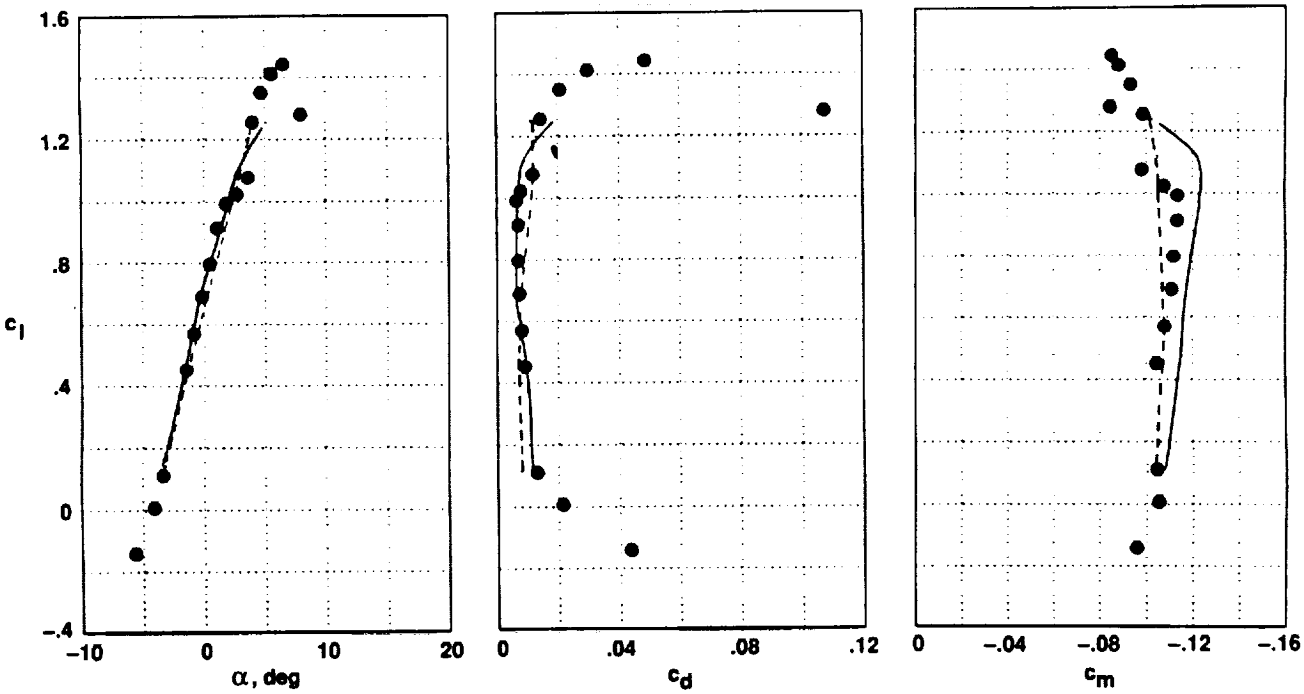

(l) M = 0.60, Re = 2,000,000

Figure 24. Concluded.

NASA
National Aeronautics and Space Administration

Report Documentation Page

1. Report No. NASA TM-102840	2. Government Accession No.	3. Recipient's Catalog No.

4. Title and Subtitle
An Evaluation of Three Two-Dimensional Computational Fluid Dynamics Codes Including Low Reynolds Numbers and Transonic Mach Numbers

5. Report Date
January 1991

6. Performing Organization Code

7. Author(s)
Raymond M. Hicks and Susan E. Cliff

8. Performing Organization Report No.
A-90202

10. Work Unit No.
505-61-21

9. Performing Organization Name and Address
Ames Research Center
Moffett Field, CA 94035-1000

11. Contract or Grant No.

13. Type of Report and Period Covered
Technical Memorandum

12. Sponsoring Agency Name and Address
National Aeronautics and Space Administration
Washington, DC 20546-0001

14. Sponsoring Agency Code

15. Supplementary Notes
Point of Contact: Raymond M. Hicks, Ames Research Center, MS 227-2
Moffett Field, CA 94035-1000
(415) 604-5656 or FTS 464-5656

16. Abstract

Full-potential, Euler, and Navier-Stokes computational fluid dynamics (CFD) codes were evaluated for use in analyzing the flow field about airfoil sections operating at Mach numbers from 0.20 to 0.60 and Reynolds numbers from 500,000 to 2,000,000. The potential code (LBAUER) includes weakly coupled integral boundary-layer equations for laminar and turbulent flow with simple transition and separation models. The Navier-Stokes code (ARC2D) uses the thin-layer formulation of the Reynolds-averaged equations with an algebraic turbulence model. The Euler code (ISES) includes strongly coupled integral boundary-layer equations and advanced transition and separation calculations with the capability to model laminar separation bubbles and limited zones of turbulent separation. The best experiment/CFD correlation was obtained with the Euler code because its boundary-layer equations model the physics of the flow better than the other two codes. An unusual reversal of boundary-layer separation with increasing angle of attack, following initial shock formation on the upper surface of the airfoil, was found in the experimental data. This phenomenon was not predicted by the CFD codes evaluated during this study.

17. Key Words (Suggested by Author(s)) Airfoil Low Reynolds number CFD Wind tunnel testing	18. Distribution Statement Unclassified-Unlimited Subject Category – 02

19. Security Classif. (of this report) Unclassified	20. Security Classif. (of this page) Unclassified	21. No. of Pages 52	22. Price A04

NASA FORM 1626 OCT 86

For sale by the National Technical Information Service, Springfield, Virginia 22161